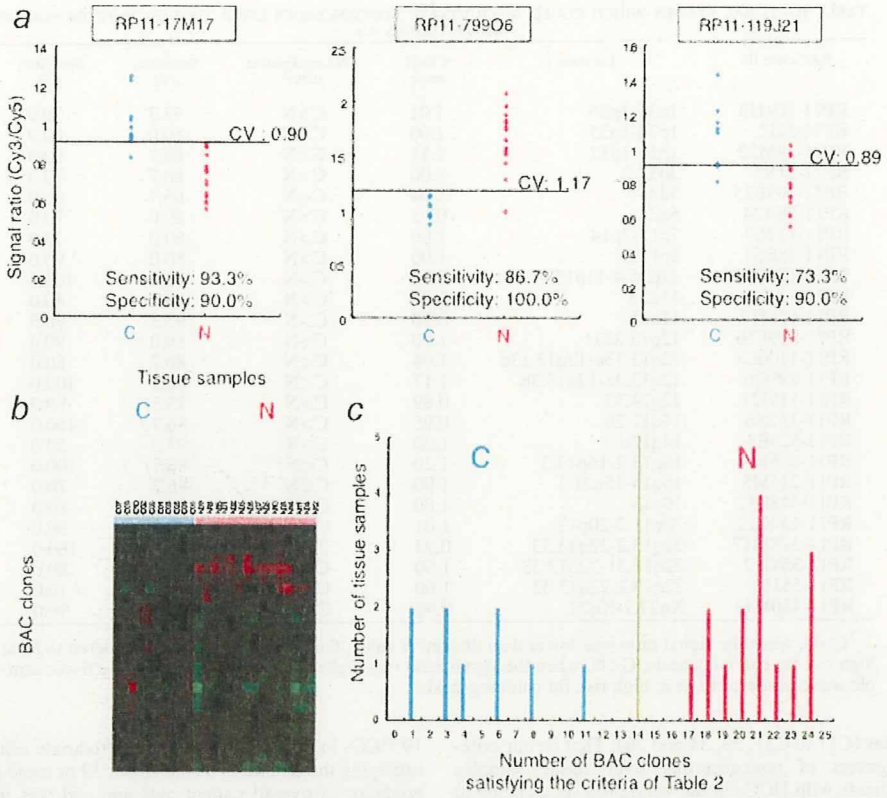

FIGURE 2 – DNA methylation profiles discriminating noncancerous liver tissue obtained from patients with HCCs from normal liver tissue. (*a*) Scattergrams of the signal ratios in normal liver tissue samples (C1 to C10) and noncancerous liver tissue samples obtained from patients with HCCs (N1 to N15) in the learning cohort on representative BAC clones, RP11-17M17, RP11-799O6 and RP11-119J21. Using the cutoff values (CV) described in each panel, noncancerous liver tissue samples obtained from patients with HCCs (N) in the learning cohort were discriminated from normal liver tissue samples (C) with sufficient sensitivity and specificity. (*b*) By 2-dimensional hierarchical clustering analysis using the 25 BAC clones selected by the process described in the Results section, normal liver tissue samples (C1 to C10) and noncancerous liver tissue samples obtained from patients with HCCs (N1 to N15) in the learning cohort were subclassified into the different subclasses without any error. The cluster trees for tissue samples and BAC clones are shown at the top and left of the panel, respectively. (*c*) Histogram showing the number of BAC clones satisfying the Table II criteria in samples C1 to C10 and N1 to N15. On the basis of this histogram, we established the following criteria: when the noncancerous liver tissue satisfied the criteria in Table II for 14 (green bar) or more than 14 BAC clones, it was judged to be at high risk of carcinogenesis.

signal ratio of HCCs did not differ from that of noncancerous liver tissue obtained from patients with HCCs (131 BAC clones). From the 512 BAC clones, 358 (Groups I, II, III and IV), in which the DNA methylation status was inherited by HCCs from noncancerous liver tissue, were selected. From the 358 BAC clones, the first 40 were identified by spot ranking analysis using the support vector machine algorithm for discrimination of noncancerous liver tissue obtained from patients with HCCs from normal liver tissue. Figure 2*a* shows scattergrams of the signal ratios in normal liver tissue samples and noncancerous liver tissue samples obtained from patients with HCCs on representative examples of the 40 BAC clones. Using the cutoff values described in each panel, noncancerous liver tissue obtained from patients with HCCs in the learning cohort was discriminated from normal liver tissue with sufficient sensitivity and specificity (Fig. 2*a*). From the 40 BAC clones, 25, for which such discrimination was performed with a sensitivity or specificity of 70% or more than 70%, were selected (Supporting Information Table S1). The cutoff values of the signal ratios for the 25 BAC clones, and their sensitivity and specificity, are shown in Table II. Two-dimensional hierarchical clustering analysis using the 25 BAC clones is shown in Figure 2*b*: 10 normal liver tissue samples (C1 to C10) and 15 noncancerous liver tissue samples obtained from patients with HCCs (N1 to N15) in the learning cohort were subclassified into different subclasses without any error. The number of BAC clones satisfying the criteria listed in Table II in noncancerous liver tissue samples showing chronic hepatitis (20.6 ± 1.8) was not significantly different from that showing cirrhosis (21.3 ± 2.4, $p = 0.542$) in the learning cohort.

A histogram showing the number of BAC clones satisfying the criteria listed in Table II for samples C1 to C10 and N1 to N15 is shown in Figure 2*c*. On the basis of this figure, we finally established the following criteria: when noncancerous liver tissue satisfied the criteria of Table II for 14 or more BAC clones (green bar in Fig. 2*c*), it was judged to be at high risk of carcinogenesis, and when noncancerous liver tissue satisfied the criteria of Table II for less than 14 BAC clones, it was judged not to be at high risk of carcinogenesis. Based on these criteria, both the sensitivity and specificity for diagnosis of noncancerous liver tissue samples obtained from patients with HCCs in the learning cohort as being at high risk of carcinogenesis were 100%.

To confirm these criteria, an additional 50 liver tissue samples were analyzed by BAMCA as a validation study (Supporting Information Figure S1). Twenty-three of 24 validation samples satisfying the criteria of Table II for 14 or more BAC clones were noncancerous liver tissue samples obtained from patients with HCCs (N16 to N36 and N38), and 24 of 26 validation samples satisfying the criteria of Table II for less than 14 BAC clones were normal

TABLE II – 25 BAC CLONES WHICH COULD DISCRIMINATE NONCANCEROUS LIVER TISSUES (N) FROM NORMAL LIVER TISSUES (C)

BAC clone ID	Location	Cutoff value	DNA methylation status[1]	Sensitivity (%)	Specificity (%)
RP11-104J13	1p35-1p36	1.01	C>N	93.3	70.0
RP11-52I2	1p34-1p35	1.00	C<N	80.0	60.0
RP11-29M22	1p11-1p12	1.11	C<N	86.7	90.0
RP11-21K1	2q37.2	1.00	C>N	86.7	70.0
RP11-109B15	5q33	1.04	C<N	66.7	90.0
RP11-88B24	6q26	0.95	C>N	80.0	70.0
RP11-112B7	7p13-7p14	1.00	C>N	80.0	70.0
RP11-48D21	8p11.2	1.00	C>N	80.0	90.0
RP11-120E20	11p15.4-11p15.5	0.90	C>N	73.3	100.0
RP11-334E6	11q23	1.00	C>N	86.7	80.0
RP11-17M17	11q25	0.90	C>N	93.3	90.0
RP11-319E16	12p13.32a	1.00	C>N	80.0	90.0
RP11-1100L3	12q13.13c-12q13.13d	1.04	C<N	86.7	80.0
RP11-799O6	12q13.3a-12q13.3b	1.17	C<N	86.7	100.0
RP11-119J21	12q24.33	0.89	C>N	73.3	90.0
RP11-332N6	14q11.2b	0.95	C>N	86.7	100.0
RP11-529E4	14q12c	1.00	C>N	93.3	50.0
RP11-89M4	16p13.2-16p13.3	1.20	C<N	86.7	100.0
RP11-215M5	15q15-15q21.1	1.00	C<N	86.7	70.0
RP11-348B12	19p13	1.00	C<N	80.0	80.0
RP11-134G22	20p11.2-20p12	1.01	C>N	80.0	90.0
RP11-328M17	22q13.2-22q13.33	0.93	C>N	86.7	100.0
RP11-354I12	22q13.31-22q13.33	1.00	C>N	93.3	80.0
RP11-55J11	22q13.2-22q13.33	1.00	C>N	80.0	70.0
RP11-480M11	Xq27.1-Xq28	0.90	C>N	80.0	90.0

[1]C>N, when the signal ratio was lower than the cutoff value, the tissue sample was considered to be at high risk for carcinogenesis; C<N, when the signal ratio was higher than the cutoff value, the tissue sample was considered to be at high risk for carcinogenesis.

liver tissue samples (C11 to C31, 33, 34 and 36). That is, our criteria enabled diagnosis of noncancerous liver tissue samples obtained from patients with HCCs in the validation set as being at high risk of carcinogenesis with a sensitivity of 95.8% and a specificity of 96.2%. The number of BAC clones satisfying the criteria listed in Table II in noncancerous liver tissue samples showing chronic hepatitis (17.6 ± 2.5) was not significantly different from that showing cirrhosis (19.4 ± 1.8, $p = 0.128$) in the validation cohort.

In addition, the average number of BAC clones satisfying the criteria in Table II was significantly lower in 7 samples of liver tissue obtained from patients who were infected with HBV or HCV, but who had never developed HCCs (V1 to V7, 13.14 ± 4.78), than that in N1 to N39 (19.21 ± 2.67, $p = 0.00419$).

Association of HCC DNA methylation profiles with patient outcome

To establish criteria for prognostication of patients with HCCs, in the learning cohort, 5 of 19 HCC samples obtained from patients who had survived more than 4 years after hepatectomy and 6 of 19 HCC samples from patients who had suffered recurrence within 6 months and died within a year after hepatectomy were defined as a favorable-outcome group and a poor-outcome group, respectively. Wilcoxon test ($p < 0.01$) revealed that the signal ratios of 41 BAC clones (Supporting Information Table S1) differed significantly between the favorable-outcome group ($n = 5$) and the poor-outcome group ($n = 6$). Figure 3*a* shows scattergrams of the signal ratios in samples from the favorable- and poor-outcome groups for representative examples of the 41 BAC clones. Using the cutoff values described in Figure 3*a* and Table III for the 41 BAC clones, samples from the poor-outcome group were discriminated from favorable-outcome group samples with sufficient sensitivity and specificity (Fig. 3*a* and Table III). Two-dimensional hierarchical clustering analysis using the 41 BAC clones is shown in Figure 3*b*: 5 HCCs in the favorable-outcome group and 6 HCCs in the poor-outcome group were subclassified into different subclasses without any error (Fig. 3*b*). A histogram showing the number of BAC clones satisfying the criteria in Table III is shown in Fig. 3*c*. In all 19 HCCs in the learning cohort, multivariate analysis revealed that satisfying the criteria in Table III for 32 or more BAC clones was a predictor of overall patient outcome and was independent of parameters that are already known to have prognostic impact,[20] such as histological differentiation, portal vein tumor thrombi, intrahepatic metastasis and multicentricity (Table IV).

To confirm these criteria, an additional 25 HCC samples were analyzed by BAMCA as a validation study, and then evaluated based on the criteria in Table III. All 44 HCCs were divided into 2 groups according to the number of BAC clones satisfying the criteria (32 or more BAC clones *vs.* less than 32 BAC clones). The period covered ranged from 11 to 3,413 days (mean, 1,349 days). The cancer-free and overall survival rates of patients with HCCs satisfying the criteria in Table III for 32 or more BAC clones was significantly lower than that of patients with HCCs satisfying the criteria in Table III for less than 32 BAC clones (Fig. 3*d*, $p = 0.000000002$ and $p = 0.0013$, respectively).

Discussion

Although many researchers in the field of cancer epigenetics use promoter arrays to identify the genes that are methylated in cancer cells,[21–23] we used a BAC array[19] in this study. The efficiency of identification of specific genes that are silenced by DNA methylations around the promoter regions and may become a target of therapy may be generally lower using the BAMCA approach than with conventional promoter array-based analysis. However, the promoter regions of specific genes are not the only target of DNA methylation alterations in human cancers. DNA methylation status in genomic regions not directly participating in gene silencing, such as the edges of CpG islands, may be altered at the precancerous stage before the alterations of the promoter regions themselves occur.[24] Moreover, aberrant DNA methylation of large regions of chromosomes, which are regulated in a coordinated manner in human cancers due to a process of long-range epigenetic silencing, has recently attracted attention.[25] BAMCA methods may be suitable for overviewing the DNA methylation status of individual large regions among all chromosomes and for

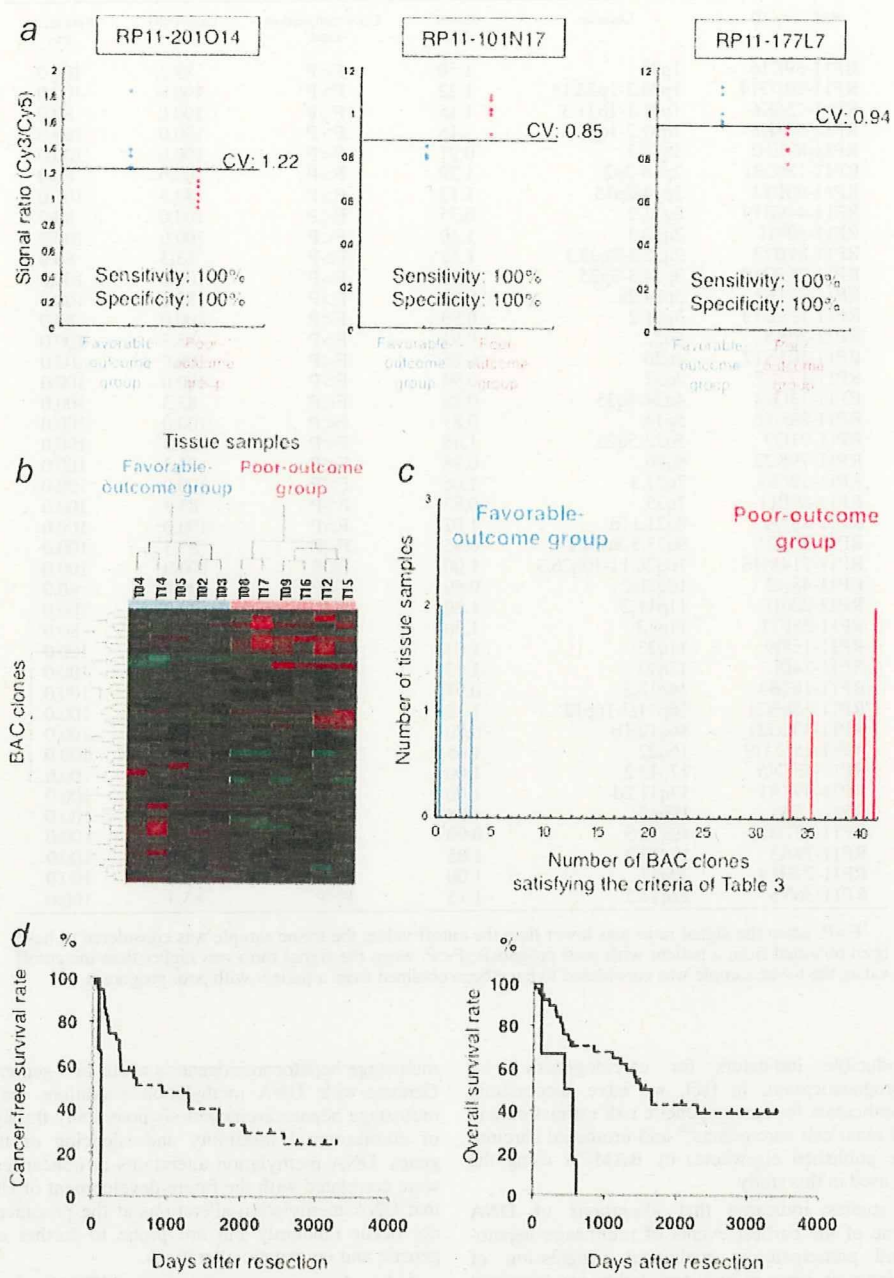

FIGURE 3 – DNA methylation profiles in HCCs associated with patient outcome. (*a*) Scattergrams of the signal ratios in HCCs from patients who survived more than 4 years after hepatectomy (favorable-outcome group, $n = 5$) and HCCs from patients who suffered recurrence within 6 months and died within a year after hepatectomy (poor-outcome group, $n = 6$) in the learning cohort for representative BAC clones, RP11-201O14, RP11-101N17 and RP11-177L7. Using the described cutoff values (CV), the poor-outcome group was discriminated from the favorable-outcome group with 100% sensitivity and specificity. (*b*) By 2-dimensional hierarchical clustering analysis using the 41 BAC clones selected by Wilcoxon test, HCCs in the favorable-outcome group and those in the poor-outcome group in the learning cohort were subclassified in the different subclasses without any error. The cluster trees for tissue samples and BAC clones are shown at the top and left of the panel, respectively. (*c*) Histogram showing the number of BAC clones satisfying the Table III criteria in HCCs of the favorable- and poor-outcome groups in the learning cohort. (*d*) Kaplan-Meier survival curves of all patients with HCCs (T1 to T44). The cancer-free (left panel, $p = 0.000000002$) and overall (right panel, $p = 0.0013$) survival rates of patients with HCCs satisfying the Table III criteria for 32 or more than 32 BAC clones (solid lines) were significantly lower than that of patients with HCCs satisfying the Table III criteria for less than 32 BAC clones (broken lines).

TABLE III – 41 BAC CLONES WHICH COULD DISCRIMINATE HCCS IN POOR-OUTCOME GROUP (P) FROM THOSE IN FAVORABLE-OUTCOME GROUP (F)

BAC clone ID	Location	Cutoff value	DNA methylation status[1]	Sensitivity (%)	Specificity (%)
RP11-89K16	1p35	1.50	F<P	83.3	100.0
RP11-201O14	1p34.3-1p36.13	1.22	F>P	100.0	100.0
RP11-156K6	1p31.1-1p31.3	1.15	F>P	100.0	80.0
RP11-553K8	1q31.2-1q31.3	1.16	F>P	100.0	100.0
RP11-89E10	1q31.3	0.91	F<P	100.0	100.0
RP11-180L21	2p16-2p21	1.29	F>P	100.0	80.0
RP11-90B13	2p14-2p15	1.13	F>P	83.3	100.0
RP11-449B19	2q11.2	0.75	F<P	100.0	80.0
RP11-30M1	2q32.3	1.10	F<P	100.0	100.0
RP11-89B13	2q32.3-2q33.1	1.11	F>P	83.3	80.0
RP11-255O19	3p24.3-3p25	1.08	F>P	100.0	100.0
RP11-421F9	3p24.2a	0.97	F>P	83.3	100.0
RP11-122D19	3p21.2	0.99	F<P	100.0	80.0
RP11-36K8	4q22	0.91	F>P	83.3	100.0
RP11-101N17	4q26	0.85	F<P	100.0	100.0
RP11-177L7	4q32	0.94	F>P	100.0	100.0
RP11-13O14	4q34-4q35	0.88	F<P	83.3	100.0
RP11-88H16	5p14	0.85	F<P	100.0	100.0
RP11-91G9	5q22-5q23	1.45	F<P	83.3	100.0
RP11-79K22	6q16	0.98	F<P	83.3	100.0
RP11-126B8	7q21.3	1.06	F>P	100.0	100.0
RP11-89P11	7q35	0.83	F>P	83.3	100.0
RP11-88N8	8q21.11d	1.02	F>P	100.0	100.0
RP11-85C21	9q33.3-9q34.2	0.95	F<P	83.3	100.0
RP11-714M16	10q26.11-10q26.3	1.00	F<P	100.0	100.0
RP11-48A2	10q26.2	0.69	F<P	100.0	80.0
RP11-206I1	11p11.2	1.20	F<P	100.0	100.0
RP11-35F11	11q12	1.30	F<P	100.0	80.0
RP11-158I9	11q23	1.04	F>P	83.3	100.0
RP11-74I8	12q13	1.13	F<P	100.0	100.0
RP11-167B4	16p13.3	0.97	F>P	83.3	100.0
RP11-368N21	16p11.2-16p12	1.10	F>P	83.3	100.0
RP11-303G21	16q12.1b	0.80	F>P	83.3	100.0
RP11-151M19	16q22	1.05	F>P	100.0	100.0
RP11-135N5	17p13.2	1.00	F>P	100.0	100.0
RP11-398A1	17q11.2d	1.00	F>P	100.0	100.0
RP11-15A1	19q13	1.08	F>P	83.3	100.0
RP11-697B10	19q13.3	0.90	F>P	83.3	100.0
RP11-79A3	19q13.3	1.05	F<P	100.0	100.0
RP11-29H19	20q12	1.00	F>P	100.0	100.0
RP11-36N5	22q11.2	1.15	F>P	83.3	100.0

[1]F>P, when the signal ratio was lower than the cutoff value, the tissue sample was considered to have been obtained from a patient with poor prognosis; F<P, when the signal ratio was higher than the cutoff value, the tissue sample was considered to have been obtained from a patient with poor prognosis.

identifying reproducible indicators for carcinogenetic risk estimation and prognostication. In fact, we have successfully obtained optimal indicators for carcinogenetic risk estimation and prognostication of renal cell carcinomas[26] and urothelial carcinomas (data will be published elsewhere) by BAMCA using the same array as that used in this study.

Our previous studies indicated that alterations of DNA methylation are one of the earliest events of multistage hepatocarcinogenesis and participate in malignant progression of HCCs.[5,7-14,27-29] However, since in previous studies we examined DNA methylation status on only a restricted number of CpG islands or chromosomal loci, it has not yet been clarified whether DNA methylation status on only restricted regions is simply altered at the precancerous stage, or whether genome-wide alterations of DNA methylation status have certain clinicopathological significance. As shown in Panel N of Figure 1*b*, genome-wide DNA methylation alterations (both hypo- and hypermethylation) were confirmed even in noncancerous liver tissue samples obtained from patients with HCCs. The number of BAC clones showing DNA methylation alterations and the degree of DNA methylation alterations were found to increase stepwise from the precancerous stage to the HCC stage (Fig. 1*b* and Table I). This study revealed that alterations of DNA methylation during multistage hepatocarcinogenesis occur in a genome-wide manner. Genome-wide DNA methylation alterations may participate in multistage hepatocarcinogenesis potentially through the induction of chromosomal instability and silencing of tumor-suppressor genes. DNA methylation alterations in noncancerous liver tissue were correlated with the future development of HCCs, suggesting that DNA methylation alterations at the precancerous stage may not occur randomly but are prone to further accumulation of genetic and epigenetic alterations.

Although mass vaccination against HBV has been initiated, this will not have a major impact for many years, as the age at presentation of HBV is older than 50 years mainly in Asia and Africa.[30] The spread of HCV in Japan that occurred in the 1950s and 1960s has resulted in a rapid increase in the incidence of HCC since 1980. In other countries including the United States, where HCV infection spread more recently, an increase in the incidence of HCC is imminent.[31] Although there were no significant differences in the number of BAC clones showing DNA hypo- or hypermethylation between HBV- and HCV-positive patients with HCCs, Wilcoxon test identified BAC clones in which DNA methylation status differed significantly between HBV- and HCV-positive patients with HCCs in both noncancerous liver tissue and cancerous tissue, suggesting that the HBV-related carcinogenetic

TABLE IV – MULTIVARIATE ANALYSIS OF CLINICOPATHOLOGICAL PARAMETERS AND DNA METHYLATION PROFILES ASSOCIATED WITH OVERALL OUTCOME IN PATIENTS WITH HCCS

Parameters	Hazard ratio (95% CI)	χ^2	p
Histological differentiation			
Well differentiated	1 (Reference)	0.031	0.8594
Moderately or poorly differentiated	0.817 (0.088-7.616)		
Portal vein tumor thrombi			
Negative	1 (Reference)	2.095	0.1478
Positive	4.474 (0.588-34.033)		
Intrahepatic metastasis[1]			
Negative	1 (Reference)	0.090	0.7647
Positive	1.248 (0.292-5.336)		
Multicentricity[1]			
Negative	1 (Reference)	1.499	0.2209
Positive	0.328 (0.055-1.955)		
The criteria of Table 3			
Satisfying for less than 32 BAC clones	1 (Reference)	4.997	0.0254
Satisfying for 32 or more BAC clones	4.466 (1.202-16.585)		

CI, confidence interval.
[1]In patients with multiple lesions, whether the lesions other than the main tumor from which tissue samples were obtained for this study were intrahepatic metastases of the main tumor or second primary lesions was judged by microscopic observation of hepatectomy specimens based on the previously described criteria.[35]

pathway may result in distinct DNA methylation profiles. These findings are in accordance with a previous report showing that HBV-related proteins can induce DNA methylation alterations.[32]

The effectiveness of surgical resection for HCC is limited, unless the disease is diagnosed early at the asymptomatic stage. Therefore, surveillance at the precancerous stage will become a priority. To reveal the baseline liver histology, microscopic examination of liver biopsy specimens is performed in patients with HBV or HCV infection prior to interferon therapy.[33,34] Therefore, carcinogenetic risk estimation using such liver biopsy specimens will be advantageous for close follow-up of patients who are at high risk of HCC development. Because even subtle alterations of DNA methylation profiles at the precancerous stage are stably preserved on DNA double strands by covalent bonds, they may be better indicators for risk estimation than mRNA and protein expression profiles that can be easily affected by the microenvironment of precursor cells.

The present genome-wide analysis revealed DNA methylation profiles that were able to discriminate noncancerous liver tissue obtained from patients with HCCs from normal liver tissue and diagnose it at high risk of HCC development in the learning set. The sensitivity and specificity in the validation set were 95.8 and 96.2%, respectively, and the criteria listed in Table II were validated. For carcinogenetic risk estimation using liver biopsy specimens obtained prior to interferon therapy, DNA methylation profiles actually associated with carcinogenesis should be discriminated from those associated with inflammation and/or fibrosis. Therefore, we first omitted potentially insignificant BAC clones associated only with inflammation and/or fibrosis and focused on BAC clones for which DNA methylation status was inherited by HCCs from the precancerous stage (Groups I, II, III and IV). In fact, it was confirmed that there were no significant differences in the number of BAC clones satisfying the criteria in Table II between noncancerous liver tissue samples showing chronic hepatitis and noncancerous liver tissue samples showing cirrhosis, not only in the learning set ($p = 0.542$) but also in the validation set ($p = 0.128$), indicating that our criteria were not associated with the degree of inflammation or fibrosis. In addition, the average numbers of BAC clones satisfying the criteria in Table II were significantly lower in liver tissue of patients without HCCs (V1 to V7) than in noncancerous liver tissue of patients with HCCs (N1 to N39), even though the patients from whom V1 to V7 were obtained were infected with HBV or HCV. Therefore, our criteria not only discriminate noncancerous liver tissue obtained from patients with HCCs from normal liver tissue but may also be applicable for classifying liver tissue obtained from patients who are followed up because of HBV or HCV infection, chronic hepatitis or cirrhosis into that which may generate HCCs and that which will not. Our criteria are applicable to both patients with chronic hepatitis and liver cirrhosis, although liver cirrhosis is known to show a more pronounced tendency to lead to HCC development than chronic hepatitis.[20] We intend to validate the reliability of such risk estimation prospectively using liver biopsy specimens obtained prior to interferon therapy from a large cohort of patients. On the basis of the present data, we now consider it justifiable to propose that clinicians can apply a portion of biopsy cores for this type of prospective study.

Because a sufficient quantity of good-quality DNA can be obtained from liver biopsy specimens, PCR-based analyses focusing on individual CpG sites are not always required. Although cut-off values should be modified for widely available standardized reference DNA, array-based analysis that overviews aberrant DNA methylation in each BAC region is immediately applicable to routine laboratory examinations. Moreover, because DNA methylation status of CpG sites is often regulated in a coordinated manner in each individual large region on chromosomes,[13,14,25] an overview of the DNA methylation tendency (hypo- or hypermethylation) in the whole BAC region can be a more reproducible diagnostic indicator than one focusing on individual CpG sites.

The present genome-wide analysis revealed DNA methylation profiles that were able to discriminate a poor-outcome group from a favorable-outcome group. Correlation between the DNA methylation profiles and both cancer-free and overall survival rates of patients with HCCs (Fig. 3*d*) validated the criteria in Table III. Prognostication based on our criteria may be promising for supportive use during follow-up after surgical resection, because multivariate analysis revealed that our criteria can predict overall patient outcome independently of parameters observed in hepatectomy specimens that are already known to have prognostic impact.[20] Such prognostication using liver biopsy specimens obtained before transarterial embolization, transarterial chemoembolization and radiofrequency ablation may be advantageous even to patients who undergo such therapies. The reliability of such prognostication needs to be validated again prospectively in surgically resected specimens or biopsy specimens.

References

1. Jones PA, Baylin SB. The fundamental role of epigenetic events in cancer. Nat Rev Genet 2002;3:415–28.
2. Gronbaek K, Hother C, Jones PA. Epigenetic changes in cancer. APMIS 2007;115:1039–59.
3. Eden A, Gaudet F, Waghmare A, Jaenisch R. Chromosomal instability and tumors promoted by DNA hypomethylation. Science 2003; 300:455.
4. Baylin SB, Ohm JE. Epigenetic gene silencing in cancer—a mechanism for early oncogenic pathway addiction? Nat Rev Cancer 2006;6:107–16.
5. Kanai Y, Ushijima S, Tsuda H, Sakamoto M, Sugimura T, Hirohashi S. Aberrant DNA methylation on chromosome 16 is an early event in hepatocarcinogenesis. Jpn J Cancer Res 1996;87: 1210–7.
6. Yoshiura K, Kanai Y, Ochiai A, Shimoyama Y, Sugimura T, Hirohashi S. Silencing of the E-cadherin invasion-suppressor gene by CpG methylation in human carcinomas. Proc Natl Acad Sci USA 1995;92:7416–9.
7. Kanai Y, Ushijima S, Hui AM, Ochiai A, Tsuda H, Sakamoto M, Hirohashi S. The E-cadherin gene is silenced by CpG methylation in human hepatocellular carcinomas. Int J Cancer 1997; 71:355–9.
8. Kanai Y, Hui AM, Sun L, Ushijima S, Sakamoto M, Tsuda H, Hirohashi S. DNA hypermethylation at the D17S5 locus and reduced HIC-1

mRNA expression are associated with hepatocarcinogenesis. Hepatology 1999;29:703–9.
9. Sun L, Hui AM, Kanai Y, Sakamoto M, Hirohashi S. Increased DNA methyltransferase expression is associated with an early stage of human hepatocarcinogenesis. Jpn J Cancer Res 1997;88:1165–70.
10. Saito Y, Kanai Y, Sakamoto M, Saito H, Ishii H, Hirohashi S. Expression of mRNA for DNA methyltransferases and methyl-CpG-binding proteins and DNA methylation status on CpG islands and pericentromeric satellite regions during human hepatocarcinogenesis. Hepatology 2001;33:561–8.
11. Saito Y, Kanai Y, Nakagawa T, Sakamoto M, Saito H, Ishii H, Hirohashi S. Increased protein expression of DNA methyltransferase (DNMT) 1 is significantly correlated with the malignant potential and poor prognosis of human hepatocellular carcinomas. Int J Cancer 2003;105:527–32.
12. Saito Y, Kanai Y, Sakamoto M, Saito H, Ishii H, Hirohashi S. Overexpression of a splice variant of DNA methyltransferase 3b, DNMT3b4, associated with DNA hypomethylation on pericentromeric satellite regions during human hepatocarcinogenesis. Proc Natl Acad Sci USA 2002;99:10060–5.
13. Kanai Y, Hirohashi S. Alterations of DNA methylation associated with abnormalities of DNA methyltransferases in human cancers during transition from a precancerous to a malignant state. Carcinogenesis 2007;28:2434–42.
14. Kanai Y. Alterations of DNA methylation and clinicopathological diversity of human cancers. Pathol Int 2008;58:544–58.
15. Gao W, Kondo Y, Shen L, Shimizu Y, Sano T, Yamao K, Natsume A, Goto Y, Ito M, Murakami H, Osada H, Zhang J, et al. Variable DNA methylation patterns associated with progression of disease in hepatocellular carcinomas. Carcinogenesis 2008; 29:1901–10.
16. Misawa A, Inoue J, Sugino Y, Hosoi H, Sugimoto T, Hosoda F, Ohki M, Imoto I, Inazawa J. Methylation-associated silencing of the nuclear receptor 1I2 gene in advanced-type neuroblastomas, identified by bacterial artificial chromosome array-based methylated CpG island amplification. Cancer Res 2005;65:10233–42.
17. Sugino Y, Misawa A, Inoue J, Kitagawa M, Hosoi H, Sugimoto T, Imoto I, Inazawa J. Epigenetic silencing of prostaglandin E receptor 2 (PTGER2) is associated with progression of neuroblastomas. Oncogene 2007;26:7401–13.
18. Tanaka K, Imoto I, Inoue J, Kozaki K, Tsuda H, Shimada Y, Aiko S, Yoshizumi Y, Iwai T, Kawano T, Inazawa J. Frequent methylation-associated silencing of a candidate tumor-suppressor. CRABP1, in esophageal squamous-cell carcinoma. Oncogene 2007;26:6456–68.
19. Inazawa J, Inoue J, Imoto I. Comparative genomic hybridization (CGH)-arrays pave the way for identification of novel cancer-related genes. Cancer Sci 2004;95:559–63.
20. Hirohashi S, Ishak KG, Kojiro M, Wanless IR, These ND, Tsukuma H, Blum HE, Deugnier Y, Puig PL, Fischer HP, Sakamoto M. Hepatocellular carcinoma. In: Hamilton SR, Altonen LA, eds. World Health Organization classification of tumours. Pathology and genetics. Tumours of the digestive system. Lyon: IARC Press, 2000. 159–72.
21. Estecio MR, Yan PS, Ibrahim AE, Tellez CS, Shen L, Huang TH, Issa JP. High-throughput methylation profiling by MCA coupled to CpG island microarray. Genome Res 2007;17:1529–36.
22. Jacinto FV, Ballestar E, Ropero S, Esteller M. Discovery of epigenetically silenced genes by methylated DNA immunoprecipitation in colon cancer cells. Cancer Res 2007;67:11481–6.
23. Nielander I, Bug S, Richter J, Giefing M, Martin-Subero JI, Siebert R. Combining array-based approaches for the identification of candidate tumor suppressor loci in mature lymphoid neoplasms. APMIS 2007;115:1107–34.
24. Maekita T, Nakazawa K, Mihara M, Nakajima T, Yanaoka K, Iguchi M, Arii K, Kaneda A, Tsukamoto T, Tatematsu M, Tamura G, Saito D, et al. High levels of aberrant DNA methylation in *Helicobacter pylori*-infected gastric mucosae and its possible association with gastric cancer risk. Clin Cancer Res 2006;12:989–95.
25. Frigola J, Song J, Stirzaker C, Hinshelwood RA, Peinado MA, Clark SJ. Epigenetic remodeling in colorectal cancer results in coordinate gene suppression across an entire chromosome band. Nat Genet 2006; 38:540–9.
26. Arai E, Ushijima S, Fujimoto H, Hosoda F, Shibata T, Kondo T, Yokoi S, Imoto I, Inazawa J, Hirohashi S, Kanai Y. Genome-wide DNA methylation profiles in both precancerous conditions and clear cell renal cell carcinomas are correlated with malignant potential and patient outcome. Carcinogenesis 2009;30:214–21.
27. Kanai Y, Ushijima S, Tsuda H, Sakamoto M, Hirohashi S. Aberrant DNA methylation precedes loss of heterozygosity on chromosome 16 in chronic hepatitis and liver cirrhosis. Cancer Lett 2000;148:73–80.
28. Kondo Y, Kanai Y, Sakamoto M, Mizokami M, Ueda R, Hirohashi S. Genetic instability and aberrant DNA methylation in chronic hepatitis and cirrhosis—A comprehensive study of loss of heterozygosity and microsatellite instability at 39 loci and DNA hypermethylation on 8 CpG islands in microdissected specimens from patients with hepatocellular carcinoma. Hepatology 2000;32:970–9.
29. Kanai Y, Saito Y, Ushijima S, Hirohashi S. Alterations in gene expression associated with the overexpression of a splice variant of DNA methyltransferase 3b, DNMT3b4, during human hepatocarcinogenesis. J Cancer Res Clin Oncol 2004;130:636–44.
30. Chang MH, Chen CJ, Lai MS, Hsu HM, Wu TC, Kong MS, Liang DC, Shau WY, Chen DS. Universal hepatitis B vaccination in Taiwan and the incidence of hepatocellular carcinoma in children. Taiwan Childhood Hepatoma Study Group. N Engl J Med 1997;336:1855–9.
31. Tanaka Y, Hanada K, Mizokami M, Yeo AE, Shih JW, Gojobori T, Alter HJ. Inaugural article: a comparison of the molecular clock of hepatitis C virus in the United States and Japan predicts that hepatocellular carcinoma incidence in the United States will increase over the next two decades. Proc Natl Acad Sci USA 2002;99:15584–9.
32. Park IY, Sohn BH, Yu E, Suh DJ, Chung YH, Lee JH, Surzycki SJ, Lee YI. Aberrant epigenetic modifications in hepatocarcinogenesis induced by hepatitis B virus X protein. Gastroenterology 2007; 132:1476–94.
33. Arase Y, Ikeda K, Suzuki F, Suzuki Y, Kobayashi M, Akuta N, Hosaka T, Sezaki H, Yatsuji H, Kawamura Y, Kobayashi M, Kumada H. Comparison of interferon and lamivudine treatment in Japanese patients with HBeAg positive chronic hepatitis B. J Med Virol 2007; 79:1286–92.
34. Yoshida H, Tateishi R, Arakawa Y, Sata M, Fujiyama S, Nishiguchi S, Ishibashi H, Yamada G, Yokosuka O, Shiratori Y, Omata M. Benefit of interferon therapy in hepatocellular carcinoma prevention for individual patients with chronic hepatitis C. Gut 2004;53:425–30.
35. Oikawa T, Ojima H, Yamasaki S, Takayama T, Hirohashi S, Sakamoto M. Multistep and multicentric development of hepatocellular carcinoma: histological analysis of 980 resected nodules. J Hepatol 2005;42:225–9.

GASTROENTEROLOGY 2009;136:2304–2315

BASIC—LIVER, PANCREAS, AND BILIARY TRACT

Disruption of *Dicer1* Induces Dysregulated Fetal Gene Expression and Promotes Hepatocarcinogenesis

SHIGEKI SEKINE,*,‡ REIKO OGAWA,* RIE ITO,* NOBUYOSHI HIRAOKA,* MICHAEL T. MCMANUS,‡ YAE KANAI,* and MATTHIAS HEBROK‡

Pathology Division, National Cancer Center Research Institute, Tokyo, Japan; and ‡Diabetes Center, Department of Medicine, University of California San Francisco, San Francisco, California

BACKGROUND & AIMS: Growing evidence suggests that microRNAs coordinate various biological processes in the liver. We describe experiments to address the physiologic roles of these new regulators of gene expression in the liver that are as of yet largely undefined. **METHODS:** We disrupted Dicer, an enzyme essential for the processing of microRNAs, in hepatocytes using a conditional knockout mouse model to elucidate the consequences of loss of microRNAs. **RESULTS:** The conditional knockout mouse livers showed the efficient disruption of *Dicer1* at 3 weeks after birth. This resulted in prominent steatosis and the depletion of glycogen storage. *Dicer1*-deficient liver exhibited increased growth-promoting gene expression and the robust expression of fetal stage–specific genes. The consequence of Dicer elimination included both increased hepatocyte proliferation and overwhelming apoptosis. Over time, *Dicer1*-expressing wild-type hepatocytes that had escaped Cre-mediated recombination progressively repopulated the entire liver. Unexpectedly, however, two thirds of the mutant mice spontaneously developed hepatocellular carcinomas derived from residual *Dicer1*-deficient hepatocytes at 1 year of age. **CONCLUSIONS: Dicer and microRNAs have critical roles in hepatocyte survival, metabolism, developmental gene regulation, and tumor suppression in the liver. Loss of Dicer primarily impairs hepatocyte survival but can promote hepatocarcinogenesis in cooperation with additional oncogenic stimuli.**

Dicer, an endoribonuclease III type enzyme, cleaves premicroRNAs and double-stranded RNAs into mature microRNAs and short interfering RNAs. Previous studies have shown that the disruption of Dicer results in the loss of mature microRNAs, indicating that Dicer is necessary for microRNA processing.[1–3] While the exact mechanisms are still under investigation, the involvement of microRNAs in the coordination of many biological processes via the regulation of messenger RNA expression and translation has been well established. Growing evidence suggests a physiologic role of microRNAs in the liver. The down-regulation of mir-122, the most abundant microRNA in hepatocytes, resulted in the suppression of cholesterol biosynthesis and the treated mice became resistant to high-fat diet–induced steatosis.[4,5] Furthermore, Grimm et al reported that the injection of a high-titer hairpin RNA expression vector into mice resulted in fatal liver dysfunction and injury.[6] These mice showed impaired microRNA processing arising from oversaturation of exportin-5–dependent microRNA transport, and the results were interpreted to suggest that microRNAs are indispensable for proper liver function and hepatocyte survival.

In addition to the roles in the regulation of physiologic functions of the liver, microRNAs are likely involved in hepatocarcinogenesis. Many microRNAs show altered expression in hepatocellular carcinomas (HCCs),[7,8] and mir-122, which targets *CCNG1*, is frequently down-regulated in HCCs.[8] However, the mechanisms by which the altered microRNA expression contributes to hepatocarcinogenesis remain largely unclear.

To elucidate the role of Dicer and microRNAs in the liver, we generated hepatocyte-specific *Dicer1* knockout mice. Because Dicer is encoded by a single locus within the mouse genome, the disruption of the single *Dicer1* gene results in the loss of all microRNAs.[1–3,9] Our findings showed that Dicer is necessary for hepatocyte survival and proper metabolic regulation. Furthermore, a significant proportion of the knockout mice spontaneously developed HCCs, providing evidence for the tumor suppressive activity of *Dicer1*.

Abbreviation used in this paper: PCR, polymerase chain reaction.

0016-5085/09/$36.00
doi:10.1053/j.gastro.2009.02.067

Materials and Methods

Mice

Alb promoter-driven Cre recombinase transgenic mice (*Albumin-Cre* mice) and mice carrying the floxed allele of *Dicer1* (*Dicer1*$^{loxP/loxP}$ mice) have been previously described.[1,10] *Albumin-Cre* and *Dicer1*$^{loxP/loxP}$ mice were crossed to obtain hepatocyte-specific *Dicer1* knockout mice (*Albumin-Cre;Dicer1*$^{loxP/loxP}$ mice). *Dicer1*$^{loxP/loxP}$ littermates were used as controls throughout the experiment. The mice used in the present study were maintained in barrier facilities according to the protocols approved by the Committee on Animal Research of the University of California San Francisco and the Committee for Ethics in Animal Experimentation at the National Cancer Center, Japan.

Histologic Analysis

Formalin-fixed and paraffin-embedded sections were subjected to H&E staining. Immunohistochemistry was performed on either paraffin-embedded or frozen sections using the avidin-biotin complex method as previously described.[11] Primary antibodies used are listed in Supplementary Table 1. Oil red O staining was performed on frozen sections fixed with formalin. Periodic acid–Schiff staining was performed on frozen sections fixed with Carnoy's fixative. Electron microscopy analysis was performed using standard procedures.

In situ hybridization against mir-122 was performed on frozen sections using locked nucleic acid probe labeled with digoxigenin (Exiqon, Vedbeak, Denmark) as previously described.[12] The signal was visualized using NBT/BCIP as a chromogen.

Serum, Blood Glucose, and Liver Lipid Analysis

Blood samples were collected from the inferior vena cava at necropsy. The serum was then separated and subjected to analysis (IDEXX, MA and SRL, Tokyo, Japan). Mouse tail vein blood glucose levels were measured using a standard glucometer. A liver lipid analysis was performed using commercially available kits (Wako, Tokyo, Japan; and Eiken, Tokyo, Japan) following methanol-chloroform extraction.

Reverse-Transcription Polymerase Chain Reaction

Reverse-transcription reaction and conventional polymerase chain reaction (PCR) were performed using standard protocols. Quantitative PCRs were performed using SYBR Green PCR Master Mix (Applied Biosystems, Foster City, CA). The expression of liver genes was compared with the expression level of *Gusb,* as previously described.[11] The primer sequences are available upon request.

Northern Blotting

Total RNA was fractioned on a 15% polyacrylamide gel, transferred to nylon membrane, and hybridized to a radiolabeled oligonucleotide complementary to mir-122.[5] Ethidium bromide staining of 5S RNA served as a control.

Microarray Analysis

Total RNA was extracted from 3 control and 3 *Albumin-Cre;Dicer1*$^{loxP/loxP}$ mice. Complementary RNA synthesis and labeling was performed using GeneChip Two-Cycle Target Labeling and Control Reagent (Affymetrix, Santa Clara, CA). Gene expression profile was assessed by GeneChip Genome 430 2.0 Array (Affymetrix) following the manufacturer's protocol. Data analysis was performed on the NIA array analysis Web site.[13] Genes that showed more than 2-fold changes with a false discovery rate <0.05 were considered significantly altered. Gene Ontology analysis was performed using the DAVID functional annotation tool.[14] Overrepresented Gene Ontology terms for biological pathways among significantly altered genes were analyzed with default settings.

MicroRNA expression was also determined for the same set of RNA samples. Samples were labeled using miRCURY LNA microRNA Power Hy3/Hy5 Labeling Kit (Exiqon) and microRNA expression profiles were assessed by miRCURY LNA version 10.0 - hsa, mmu & rno (Exiqon). MicroRNAs that showed more than 2-fold changes with a false discovery rate <0.05 were considered significantly altered.

Western Blotting

Western blotting was performed as previously described.[11] Primary antibodies used are listed in Supplementary Table 1.

Statistical Analysis

The results are presented as mean ± SD. Statistical significance was determined by Student 2-tailed t test, with a P value of $<.05$ considered significant.

Results

Efficient Deletion of Dicer1 *in Young* Albumin-Cre;Dicer1$^{loxP/loxP}$ *Mouse Liver Is Followed by Repopulation With* Dicer1*-Expressing Hepatocytes*

Albumin-Cre transgenic mice and *Dicer1*$^{loxP/loxP}$ mice were crossed to achieve the hepatocyte-specific disruption of *Dicer1*.[1,10] *Albumin-Cre;Dicer1*$^{loxP/loxP}$ mice were born at the expected Mendelian ratio and survived to adulthood with no obvious growth phenotypes. An examination of *Albumin-Cre;Dicer1*$^{loxP/loxP}$ mice and their control littermates during young adulthood revealed apparent defects in liver morphology (Figure 1*A*). Three-week-old *Albumin-Cre;Dicer1*$^{loxP/loxP}$ mouse livers were homogenously pale

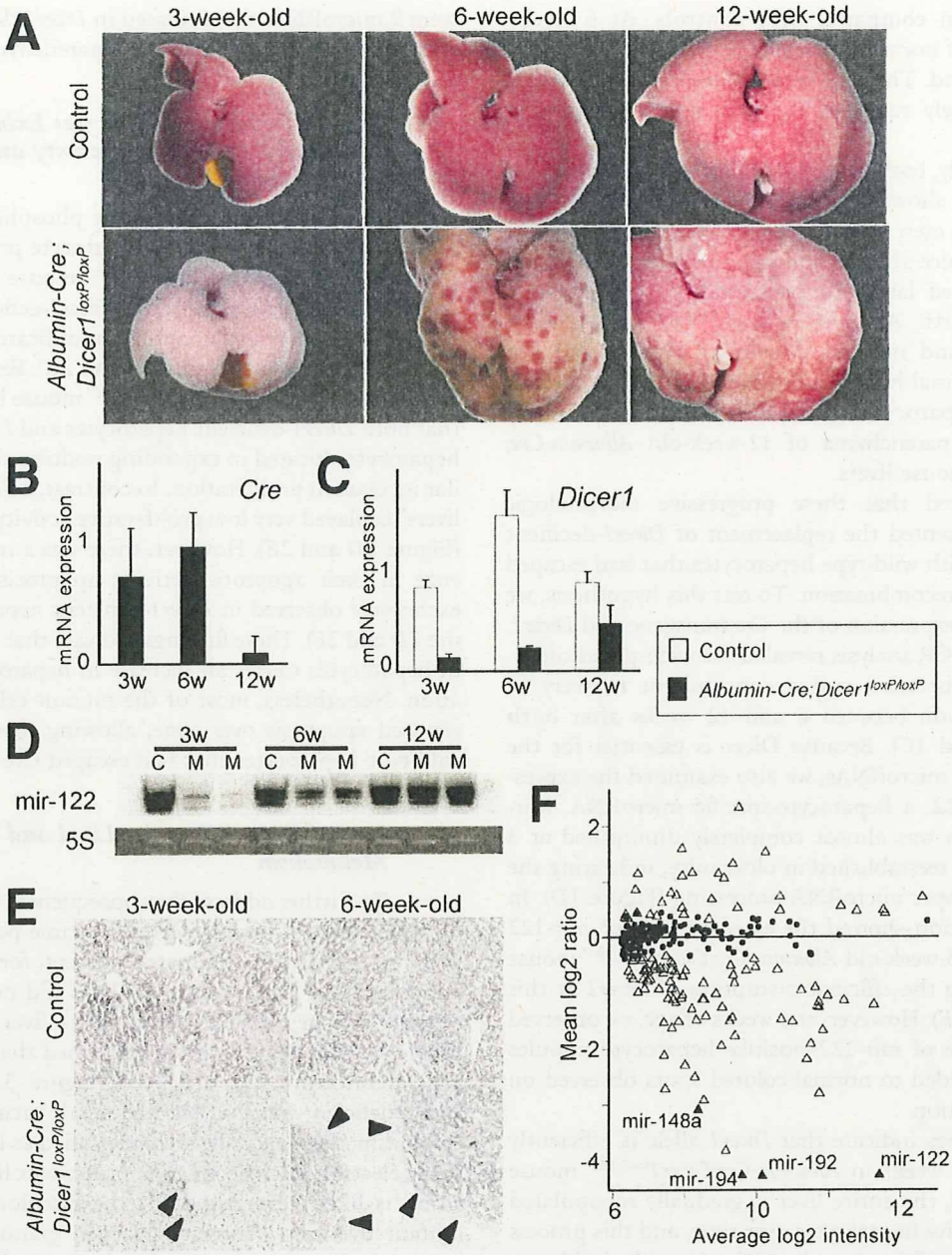

Figure 1. Efficient deletion of *Dicer1* in young *Albumin-Cre;Dicer1*$^{loxP/loxP}$ mouse liver and repopulation with *Dicer1*-expressing hepatocytes. (*A*) Gross morphology of control and *Albumin-Cre;Dicer1*$^{loxP/loxP}$ mouse livers at 3, 6, and 12 weeks after birth. At 3 weeks, the *Albumin-Cre;Dicer1*$^{loxP/loxP}$ mouse liver was pale compared with the control. At 6 weeks, the *Albumin-Cre;Dicer1*$^{loxP/loxP}$ liver had become yellowish, with the appearance of normal-colored spots. The normal-colored areas had expanded at 12 weeks. (*B*) Quantitative PCR analysis of *Cre* transgene expression in *Albumin-Cre;Dicer1*$^{loxP/loxP}$ mouse liver. (*C*) Quantitative PCR analysis of *Dicer1* expression. *Dicer1* expression recovered with age. (*D*) Northern blotting for mir-122. Ethidium bromide staining of 5S RNA was used as a loading control. C, control; M, mutant (*Albumin-Cre;Dicer1*$^{loxP/loxP}$). (*E*) In situ hybridization for mir-122. Mir-122 expression was determined in control and *Albumin-Cre;Dicer1*$^{loxP/loxP}$ mouse livers at 3 and 6 weeks of age. Livers from control mice showed diffuse expression of mir-122. Hepatocytes in the 3-week-old *Albumin-Cre;Dicer1*$^{loxP/loxP}$ mouse liver did not express mir-122 except for a few cells (*arrowheads*). Nodules of mir-122–positive hepatocytes (*arrowheads*) appeared in the 6-week-old *Albumin-Cre; Dicer1*$^{loxP/loxP}$ mouse liver. (*F*) Expression of microRNAs in 3-week-old *Albumin-Cre;Dicer1*$^{loxP/loxP}$ mouse livers. Relative expression levels of mouse microRNAs were determined in comparison with control mouse livers. MicroRNAs with significantly altered expression (false discovery rate <0.5) are represented by *open* and *black triangles*. Four previously reported liver-specific microRNAs are indicated by *black triangles*. *Black dots* indicate microRNAs without significant alteration.

in color when compared with controls. At 6 weeks, small spots of normal color had appeared on a yellowish background. These normal-colored areas expanded and had largely replaced the liver at 12 weeks after birth.

Histologically, both control and *Albumin-Cre;Dicer1*$^{loxP/loxP}$ mouse livers showed homogeneous appearance at 3 weeks of age, even though hepatocytes of *Albumin-Cre;Dicer1*$^{loxP/loxP}$ mice showed abnormalities at cytologic levels as described later (Supplementary Figure 1). At 6 weeks after birth, *Albumin-Cre;Dicer1*$^{loxP/loxP}$ mouse livers displayed round nodules consisting of enlarged but otherwise normal hepatocytes. The nodules of normal-appearing hepatocytes further expanded and largely replaced the parenchyma of 12-week-old *Albumin-Cre;Dicer1*$^{loxP/loxP}$ mouse livers.

We suspected that these progressive morphologic changes represented the replacement of *Dicer1*-decifient hepatocytes with wild-type hepatocytes that had escaped Cre-mediated recombination. To test this hypothesis, we examined the expression of the *Cre* transgene and *Dicer1*. Quantitative PCR analysis revealed the widespread silencing of *Cre* expression and a concomitant recovery of *Dicer1* expression between 6 and 12 weeks after birth (Figure 1*B* and 1*C*). Because Dicer is essential for the maturation of microRNAs, we also examined the expression of mir-122, a hepatocyte-specific microRNA. Mir-122 expression was almost completely diminished at 3 weeks but was reestablished in older mice, indicating the recovery of proper microRNA processing (Figure 1*D*). In situ hybridization showed the extensive loss of mir-122 expression in 3-week-old *Albumin-Cre;Dicer1*$^{loxP/loxP}$ mouse livers, ensuring the efficient disruption of *Dicer1* at this stage (Figure 1*E*). However, at 6 weeks of age, we observed the appearance of mir-122–positive hepatocyte nodules that corresponded to normal-colored spots observed on gross examination.

These findings indicate that *Dicer1* allele is efficiently disrupted at 3 weeks in *Albumin-Cre;Dicer1*$^{loxP/loxP}$ mouse livers; however, the entire liver is gradually repopulated by *Dicer1*-positive hepatocytes over time, and this process is achieved by nodular growth of *Dicer1*-positive wild-type hepatocytes. We did not observe oval/stem cell marker expression, including cytokeratin 19, CD34, and A6 antigen, in *Dicer1*-positive hepatocyte nodules during this process (data not shown), suggesting that liver progenitor cells do not contribute to the repopulation process.

We also assessed microRNA expression in 3-week-old *Albumin-Cre;Dicer1*$^{loxP/loxP}$ mouse livers using microarray (Figure 1*F*). The analysis identified 45 microRNAs down-regulated more than 2-fold with a false discovery rate <0.05 in *Dicer1*-deficient livers (Supplementary Tables 2 and 3). Remarkably, all 4 previously reported liver-specific microRNAs (mir-122, -148a, -192, and -194) showed robust down-regulation in *Dicer1*-deficient livers.[15] There were 9 microRNAs up-regulated in *Dicer1*-deficient livers; they are likely expressed by nonparenchymal cells and reflect secondary effects.

Dicer1-*Deficient Hepatocytes Exhibit Increased Proliferative Activity and Overwhelming Apoptosis*

Immunohistochemistry for phospho-histone H3 revealed a modest increase in hepatocyte proliferation in 3-week-old *Albumin-Cre;Dicer1*$^{loxP/loxP}$ mouse livers (Figure 2*A* and 2*B*). At the same time, *Dicer1*-deficient hepatocytes showed increased apoptosis as indicated by staining for cleaved caspase-3 (Figure 2*A* and 2*C*). Examination of 6-week-old *Albumin-Cre;Dicer1*$^{loxP/loxP}$ mouse livers revealed that both *Dicer1*-deficient hepatocytes and *Dicer1*-positive hepatocytes located in expanding nodules showed a similar increase in proliferation. In contrast, wild-type mouse livers displayed very low proliferative activity at this stage (Figure 2*D* and 2*E*). However, there was a marked difference in their apoptotic activity; apoptosis was almost exclusively observed in *Dicer1*-deficient hepatocytes (Figure 2*D* and 2*F*). These findings indicate that loss of *Dicer1* in hepatocytes causes an increase in hepatocyte proliferation. Nonetheless, most of the mutant cells are lost to elevated apoptosis over time, allowing repopulation by wild-type hepatocytes that had escaped Cre-mediated recombination.

Loss of Dicer1 *Impairs Lipid and Glucose Metabolism*

To further address the consequences of Dicer loss, we characterized 3-week-old mice, a time point at which *Dicer1* is efficiently eliminated. Except for some alterations in lipid levels, serum analyses did not reveal significant changes that would indicate liver dysfunction (Table 1). Histologic analysis confirmed that the normal liver architecture was preserved (Figure 3*A*). However, *Dicer1*-deficient hepatocytes had small vacuoles in their cytoplasm; these vacuoles were identified as lipid droplets using electron microscopy. The prominent lipid accumulation is likely responsible for the discoloration of the mutant livers. In contrast, glycogen granules normally present in hepatocytes were barely detectable in *Dicer1*-deficient hepatocytes. These findings were confirmed using histochemical analysis; oil red O staining confirmed the presence of numerous lipid droplets, and periodic acid–Schiff staining showed the depletion of glycogen in *Dicer1*-deficient hepatocytes. A detailed analysis of the lipid composition revealed a remarkable elevation of cholesterol ester and triglyceride levels, whereas the free cholesterol and free fatty acid levels were mildly increased (Figure 3*B*–*E*). Our studies also revealed that the depletion of glycogen storage led to impaired blood glucose maintenance. *Albumin-Cre;Dicer1*$^{loxP/loxP}$ mice kept on normal feeding showed only a mild decrease in their glucose levels; however, the mutant mice became severely hypoglycemic after 6 hours of fasting (Figure 3*F*). Thus, Dicer

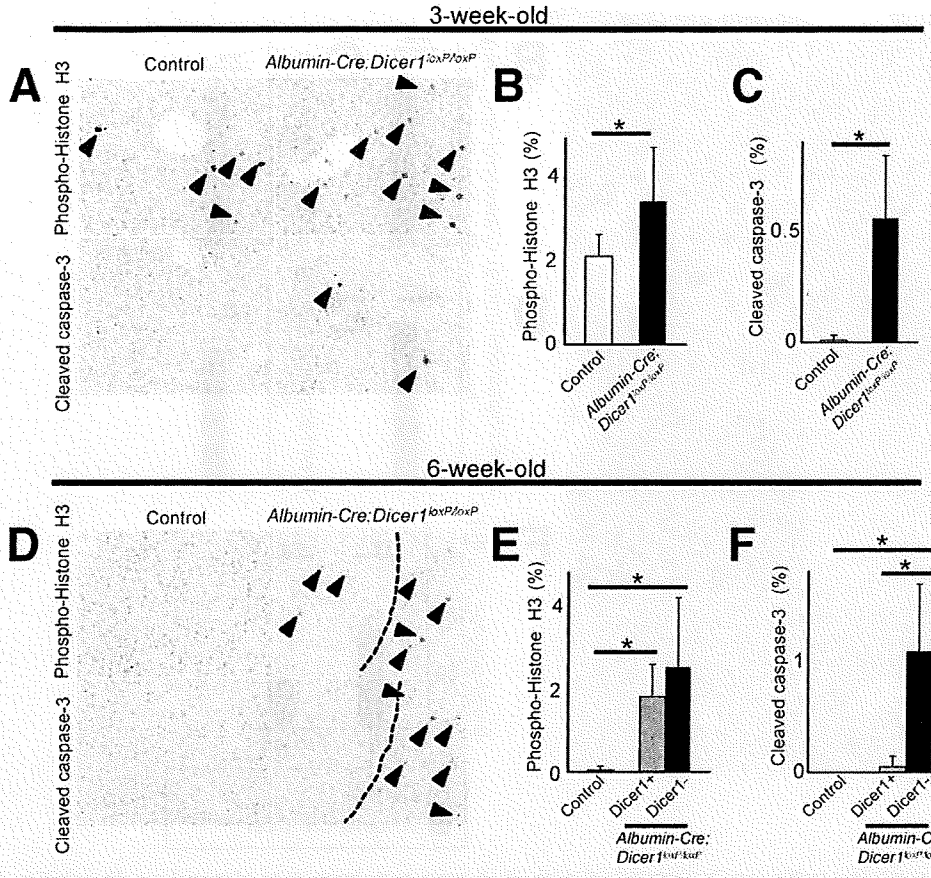

Figure 2. Increased hepatocyte proliferation and apoptosis in *Dicer1*-deficient hepatocytes. (*A* and *D*) Immunohistochemistry for phospho-histone H3 and cleaved caspase-3 in (*A*) 3-week-old and (*D*) 6-week-old mouse livers. *Dotted lines* in 6-week-old *Albumin-Cre;Dicer1*$^{loxP/loxP}$ mouse livers indicate borders between *Dicer1*-positive hepatocyte nodules (*left side*) and *Dicer1*-negative areas (*right side*). (*B*, *C*, *E*, and *F*) Quantification of hepatocyte proliferation and apoptosis in *Albumin-Cre;Dicer1*$^{loxP/loxP}$ mouse livers (n = 4–7 for each group). At least 1000 cells were counted for quantification of phospho-histone H3 and cleaved caspase-3–positive hepatocytes. For 6-week-old *Albumin-Cre;Dicer1*$^{loxP/loxP}$ *mice*, hepatocytes in *Dicer1*-positive (*gray columns*) and *Dicer1*-negative (*black columns*) areas were separately examined. $^{*}P < .05$.

function is critical for the regulation of liver lipid and glucose metabolism.

We also examined changes in the nonparenchymal cell population. Sinusoidal endothelial cells and portal tracts, including bile ducts, were not significantly altered (Supplementary Figure 2*A*). Some hematopoietic cell colonization was observed in *Dicer1*-deficient livers, and the presence of megakaryocytes and erythroblasts was confirmed by immunohistochemistry (Supplementary Figure 2*B*). In contrast, hematopoietic cells are completely absent at 3 weeks of age in control littermates. While the liver is a place for hematopoiesis during fetal stages, the liver normally loses the capacity to support hematopoiesis around the perinatal stage. The persistent presence of hematopoietic cells may represent an immature differentiation state of *Dicer1*-deficient liver.

Table 1. Metabolic Measurements of 3-Week-Old *Albumin-Cre;Dicer1*$^{loxP/loxP}$ Mice

	Control mice	*Albumin-Cre; Dicer1*$^{loxP/loxP}$ mice	*P* value
Alanine aminotransferase (*U/L*)	40.0 ± 17.0	45.6 ± 24.8	.70
Aspartate aminotransferase (*U/L*)	104.5 ± 60.2	136.6 ± 82.8	.52
γ-Glutamyl transpeptidase (*U/L*)	3.0 ± 3.8	3.4 ± 1.5	.85
Albumin (*g/dL*)	2.7 ± 0.4	2.6 ± 0.4	.83
Total protein (*g/dL*)	4.8 ± 0.3	4.0 ± 0.9	.14
Direct bilirubin (*mg/dL*)	0.1 ± 0.1	0.1 ± 0.1	.65
Indirect bilirubin (*mg/dL*)	0.0 ± 0.0	0.2 ± 0.1	.053
Triglyceride (*mg/dL*)	46.3 ± 11.8	32.6 ± 19.0	.22
Free fatty acid (*μEq/L*)	553.8 ± 156.3	1065 ± 333.2	.023
Cholesterol ester (*mg/dL*)	56.3 ± 7.0	41.6 ± 3.4	.017
Free cholesterol (*mg/dL*)	18.3 ± 1.0	58.6 ± 13.6	.0026

NOTE. n = 4–5 for each group.

Dysregulated Expression of Fetal Stage–Specific Genes in Dicer1*-Deficient Livers*

We next sought to determine whether *Dicer1*-deficient hepatocytes retain their terminally differentiated mature phenotypes. Quantitative PCR analysis revealed that the expression of liver-enriched transcription factors was maintained, with *Onecut1* and its direct target gene *Hnf1b* up-regulated significantly in *Dicer1*-deficient livers[16] (Figure 4*A*). *Hnf1a* and *Cebpb* also showed minor changes in expression levels. To further determine the differentiation status of *Dicer1*-deficient hepatocytes, we examined the expression of a battery of developmentally regulated genes. This analysis revealed dysregulated ex-

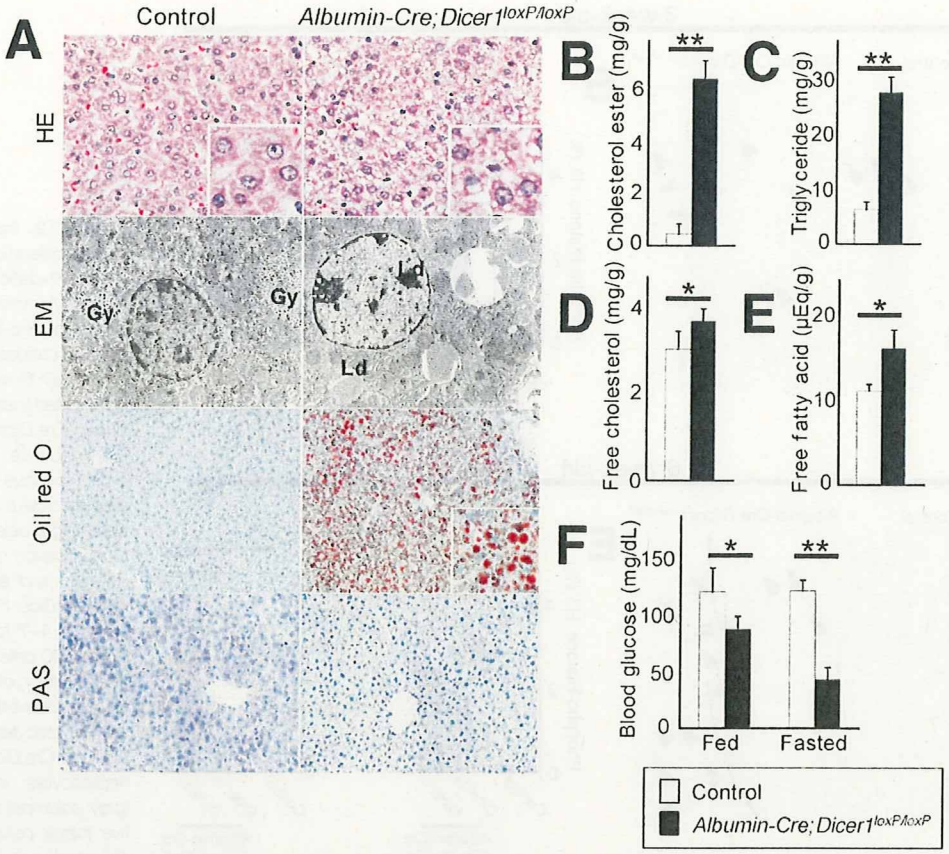

Figure 3. Impaired lipid and glucose metabolism in *Albumin-Cre;Dicer1*$^{loxP/loxP}$ mice. (*A*) Histology and ultrastructure of control and *Albumin-Cre;Dicer1*$^{loxP/loxP}$ mouse livers. Hepatocytes of control mice displayed uniform eosinophilic cytoplasm and were arranged in a trabecular pattern. The liver architecture was preserved in the *Albumin-Cre;Dicer1*$^{loxP/loxP}$ mice, but the hepatocytes exhibited small cytoplasmic vacuoles. Electron microscopy analysis of *Dicer1*-deficient hepatocytes revealed a lack of glycogen granules that are readily observed in control hepatocytes (Gy). Instead, the *Dicer1*-deficient hepatocytes contained an abundance of lipid droplets (Ld). Lipid accumulation was barely detectable in the control liver, whereas numerous lipid droplets were visible in *Dicer1*-deficient liver by oil red O staining. Periodic acid–Schiff staining highlighted glycogen in the control liver but not in the *Dicer1*-deficient liver. (*B–E*) Lipid analysis of the liver. The lipid composition of the liver tissue was determined following methanol/chloroform extraction. (*F*) Blood glucose analysis. Tail vein blood glucose level was measured in a fed condition or after 6 hours of starvation. n = 4–5 for each group. $^{*}P < .05$; $^{**}P < .0001$.

pression of genes that mark immature hepatocytes, whereas the expression pattern of genes normally found in mature hepatocytes was preserved (Figure 4*B*). The latter genes included *Sdh* and *Tdo*, which are activated during the terminal stages of liver development. Thus, with some quantitative alterations, the fundamental hepatocyte transcriptional programs of mature hepatocytes were maintained in the absence of *Dicer1*. However, Dicer function is required to repress the fetal gene expression program in adult liver.

Dicer1-*Deficient Livers Show Increased Expression of Cell Cycle–Promoting Genes and Suppression of Genes for Steroid Biosynthesis*

To define global changes in gene expression, we conducted a complementary DNA microarray analysis. The analysis generated a list of genes with more than 2-fold changes, including 1415 up-regulated and 944 down-regulated genes, that was analyzed for the enrichment in Gene Ontology categories to identify biological pathways regulated by *Dicer1*. The most enriched Gene Ontology term among the overexpressed genes was "cell division" ($P = 8.2 \times 10^{-13}$). A list of growth-promoting genes, including those encoding cyclins and aurora kinases, was found to be up-regulated in the *Dicer1*-deficient livers (Table 2). The Gene Ontology term most overrepresented among down-regulated genes was "steroid biosynthesis" ($P = 1.6 \times 10^{-15}$; Table 2). Of note, 2 previous studies using antisense oligonucleotide have shown that genes for cholesterol synthesis were down-regulated in the absence of mir-122.[4,5] In addition, we observed that previously identified direct targets of mir-122 were up-regulated modestly in *Dicer1*-deficient liver (Figure 4*C*).

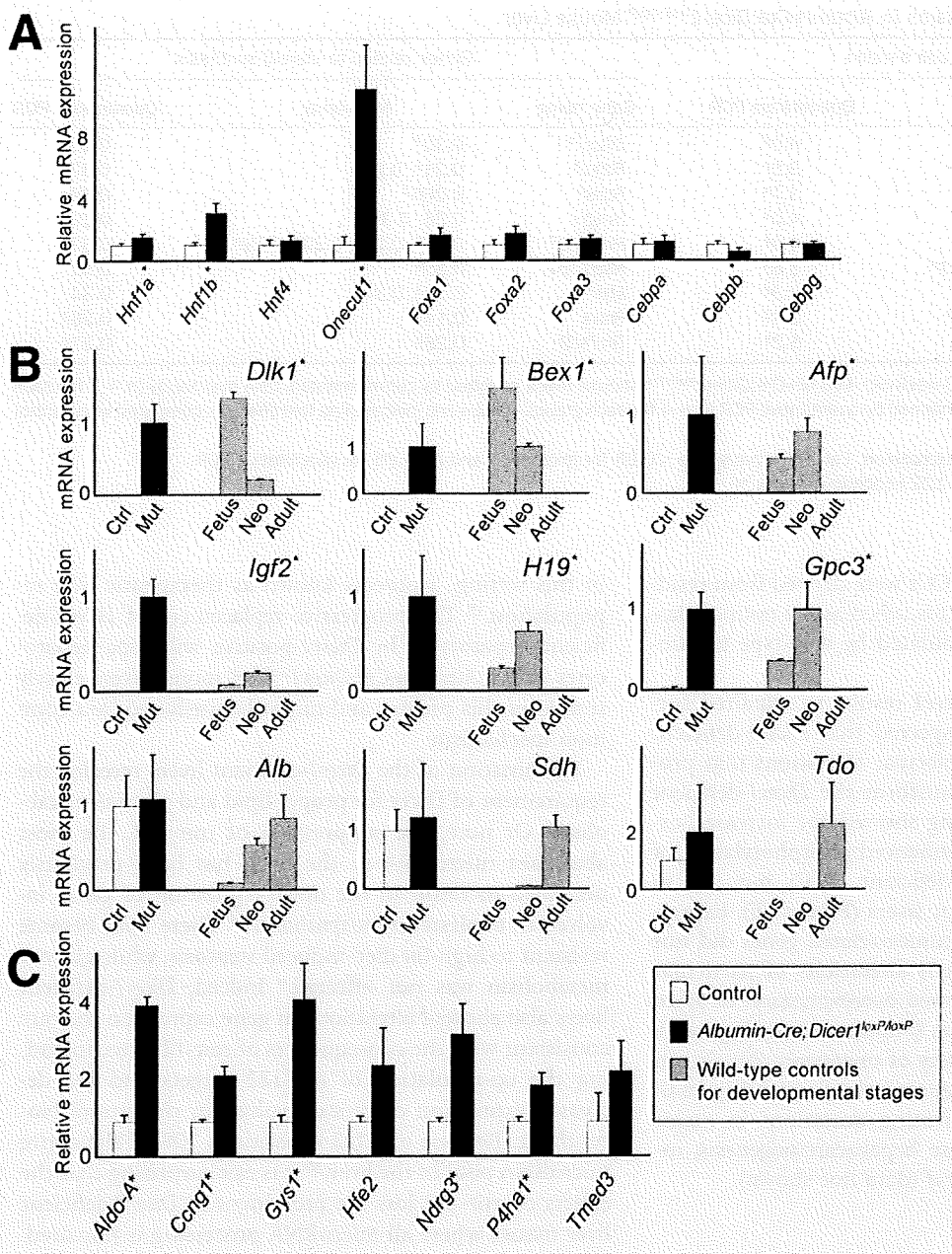

Figure 4. Expression of liver-enriched transcription factors, developmentally regulated genes, and mir-122 target genes in *Dicer1*-deficient livers. (*A*) Relative expression levels of liver-enriched transcription factors. Quantitative PCR analysis of liver samples from *Albumin-Cre;Dicer1*$^{loxP/loxP}$ and control littermates at 3 weeks after birth (n = 4 for each group). (*B*) The expression of developmentally regulated genes in control and *Albumin-Cre;Dicer1*$^{loxP/loxP}$ mice at 3 weeks (n = 5 for each group). The expression levels of wild-type mouse livers at different developmental stages were used as references (n = 3 for each group). (*C*) Expression of putative direct targets of mir-122 in *Albumin-Cre;Dicer1*$^{loxP/loxP}$ mouse livers (n = 4 for each group). Values are shown as mean ± SD. *$P <$ .05. Ctrl, control; Mut, mutant (*Albumin-Cre;Dicer1*$^{loxP/loxP}$ mice); fetus, embryonic day 14 fetus; Neo, postnatal day 0 neonate; Adult, postnatal day 42 adult.

Development of HCC in Albumin-Cre;Dicer1$^{loxP/loxP}$ *Mice*

Given that *Dicer1*-deficient hepatocytes were mostly replaced by wild-type cells at 12 weeks after birth, we were surprised to observe that one third of *Albumin-Cre;Dicer1*$^{loxP/loxP}$ mice developed HCCs after 6 months (Figure 5*A*–*C*). Furthermore, 12-month-old mice showed increased tumor incidence and progression of the disease, including 3 mice that died of tumors at 9–11 months. However, none of the mice developed metastatic lesions. Similarly to human HCCs, these tumors exhibited considerable histologic variations, including trabecular, pseudoglandular, and solid arrangements with variable degrees of steatosis (Figure 5*B*).

Remarkably, the tumors exhibited a decreased expression of *Dicer1*, persistent *Cre* transgene expression, a lack of mir-122 expression, and high expression levels of fetal liver genes (Figure 6*A*–*D*). Nonneoplastic areas consisted exclusively of histologically normal hepatocytes without evidence of preneoplastic or dysplastic changes (data not shown). In addition, nonneoplastic liver tissues obtained from tumor-bearing mice had lost *Cre* expression and were positive for *Dicer1* and mir-122 at levels comparable to those in the control littermates (Figure 6*A*–*C*). These

Table 2. Altered Gene Expression in *Albumin-Cre;Dicer1$^{loxP/loxP}$* Mouse Liver

Genes related to cell division			Genes related to steroid synthesis		
Gene name	Microarray	Quantitative PCR	Gene name	Microarray	Quantitative PCR
Aurka	2.8[a]	4.0[a]	*Dhcr7*[b]	0.30[a]	0.29[a]
Aurkb	2.2, 2.5[a]	3.5[a]	*Fdft1*[b]	0.21[a], 0.28[a]	0.37[a]
Ccna2	2.4[a], 2.6[a]	3.7[a]	*Fdps*[b]	0.066[a]	0.09[a]
Ccnb1	2.8[a], 3.0[a]	4.0[a]	*Hmgcr*	0,36, 0.39	0.29
Ccnb2	3.0[a]	4.0[a]	*Hmgcs1*[b]	0.18[a], 0.22[a], 0.22[a], 0.29[a]	0.37[a]
Ccnd1	2.8[a], 3.1[a], 3.1[a]	3.8[a]	*Hsd17b7*	0.35[a]	0.51
Ccng1[b]	2.2[a]	2.3[a]	*Mvk*[b]	0.14[a], 0.34[a]	0.34
E2f5	0.7, 1.5, 2.0[a]	2.4[a]	*Pmvk*	0.14[a]	0.25[a]
Plk1	3.6[a]	5.2[a]	*Tm7sf2*	0.28[a]	0.27[a]

NOTE. Gene expression levels of 3-week-old *Albumin-Cre;Dicer1$^{loxP/loxP}$* mouse livers analyzed by complementary DNA microarray (n = 3 for each group); the results were further confirmed by quantitative PCR (n = 4 for each group). Values are indicated as fold changes compared with control mouse livers.

[a]Genes with significantly altered expression. False discovery rate <0.05 for microarray and $P < .05$ for quantitative PCR.

[b]Significantly altered genes in mir-122 knockdown study.[4,5]

findings indicate that the HCCs were derived from residual *Dicer1*-deficient hepatocytes, whereas the nonneoplastic areas were entirely repopulated by wild-type hepatocytes.

Because disruption of *Dicer1* results in impaired survival of hepatocytes, we suspected that *Dicer1*-deficient HCCs harbor additional molecular alterations that protect from apoptosis and transform the *Dicer1*-deficient hepatocytes. Western blotting showed the increased expression of Erk1/2 and the enhanced phosphorylation of Erk1/2 and Akt in *Dicer1*-deficient HCCs but not in *Dicer1*-deficient nonneoplastic livers (Figure 6*E*). Expression analysis of a panel of tumor-related genes did not identify robust and consistent alterations of particular oncogenes in HCCs but showed overexpression of *Mycn* and *Bcl2* in a subset of tumors (Supplementary Figure 3). This may suggest that a variety of oncogenic signals can transform *Dicer1*-deficient hepatocytes. Sequencing analysis did not reveal any activating mutations in major oncogenes involved in mouse hepatocarcinogenesis, including *Ctnnb1*, *Hras*, and *Braf* (data not shown).

Discussion

Our findings indicate that the loss of *Dicer1* compromises hepatocyte survival in vivo. As indicated by the almost complete loss of mir-122, the *Alb* promoter-mediated expression of Cre recombinase in hepatocytes achieved the efficient disruption of *Dicer1* in the liver at 3 weeks after birth. However, *Dicer1*-deficient hepatocytes exhibited increased apoptosis and wild-type hepatocytes that had escaped the Cre-mediated recombination of *Dicer1* gradually repopulated the entire liver in the absence of progenitor cell expansion. Previous studies have noted that wild-type hepatocytes can display a selective growth advantage over hepatocytes with metabolic defects in vivo.[17,18] A small number of donor wild-type hepatocytes can repopulate a metabolically defective liver in this setting, a process known as therapeutic liver repopulation.[19] The progressive replacement of *Dicer1*-deficient hepatocytes by *Dicer1*-positive wild-type hepatocytes in the *Albumin-Cre;Dicer1$^{loxP/loxP}$* mouse livers closely simulates this process and might be mediated by a common mechanism.

Examination of the *Dicer1*-deficient livers revealed the requirement of Dicer for proper lipid and glucose metabolism. Of note, the suppression of mir-122, the most abundant microRNA in the liver, has been previously described to result in the down-regulation of genes involved in cholesterol biosynthesis.[4,5] These mice became resistant to high-fat diet–induced steatosis, while glucose metabolism was not affected.[4] Indeed, *Dicer1*-deficient livers also showed alterations in gene expression that are consistent with the consequences of mir-122 loss, including the up-regulation of mir-122 targets and the decreased expression of genes involved in cholesterol biosynthesis. Because mir-122 constitutes 70% of the entire microRNA pool in the liver,[20] it is not surprising that the effects of mir-122 loss are prominent in *Dicer1*-deficient liver tissues where all microRNA processing is impaired. However, in contrast to the findings obtained in the mir-122 knockdown study, the disruption of *Dicer1* resulted in marked steatosis, indicating that Dicer regulates lipid metabolism through a mir-122–dependent as well as a mir-122–independent pathway. This suggests the presence of microRNAs other than mir-122 that play critical roles in metabolic regulation in the liver. Because loss of Dicer impacts expression of a large number of genes, it is difficult to identify a specific pathway responsible for the steatosis in *Dicer1*-deficient livers. Further studies, including modulation of single microRNAs, would be required to clarify the mir-122–independent mechanisms for the regulation of lipid and glucose metabolism in the liver.

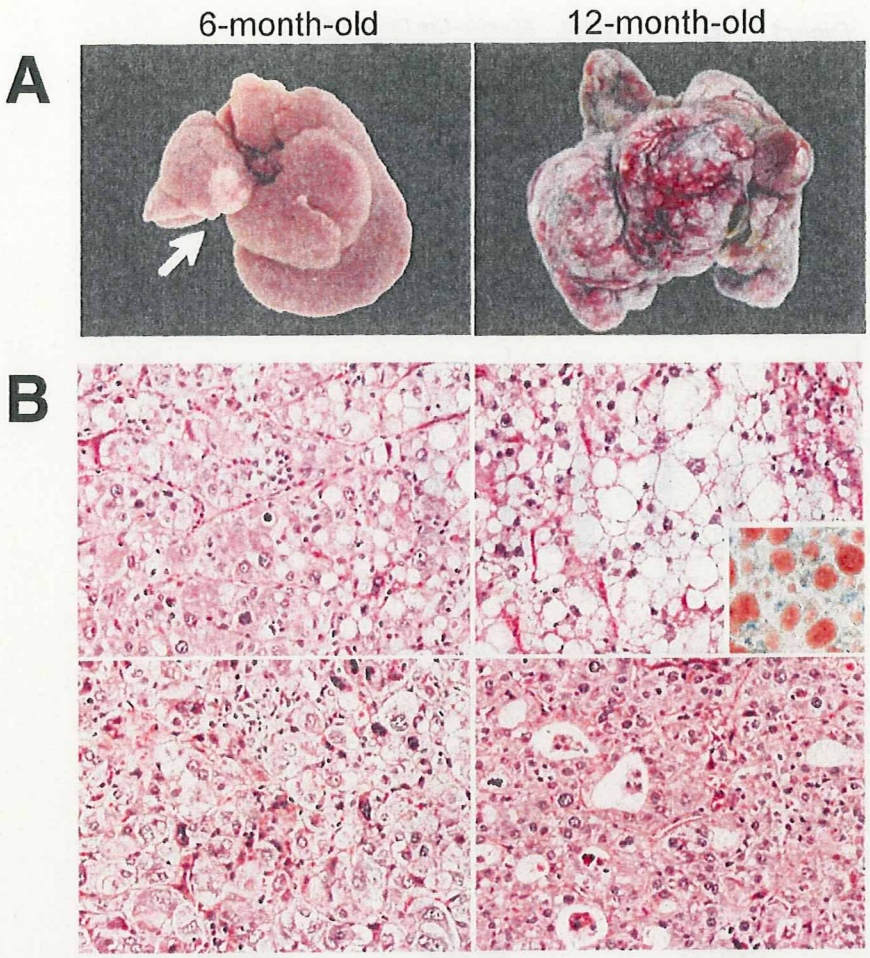

C

	6-month-old		12-month-old	
	Control	*Alb-Cre;Dicer(fl/fl)*	Control	*Alb-Cre;Dicer(fl/fl)*
Mice examined	20 M:F = 14:6	41 M:F = 12:29	19 M:F = 11:8	21 M:F = 9:12
Mice with tumors	0	15 (36.5%) M:F = 7:8	0	14 (66.7%) M:F = 6:8
Tumor size		2-20mm Average 5.5mm		2-25mm
Tumor number		1-5 Average 1.76		1-numerous

Figure 5. Development of HCC in *Albumin-Cre;Dicer1*$^{loxP/loxP}$ mice. (*A*) HCCs in *Albumin-Cre;Dicer1*$^{loxP/loxP}$ mice at 6 and 12 months after birth. A single tumor was observed in a 6-month-old *Albumin-Cre;Dicer1*$^{loxP/loxP}$ mouse liver (*left*, *arrow*). A 12-month-old *Albumin-Cre;Dicer1*$^{loxP/loxP}$ mouse liver carried multiple tumors that had replaced the liver parenchyma (*right*). (*B*) Histologic spectrum of HCCs included thick trabecular arrangement with mild steatosis (*top*, *left*), prominent steatosis (*top*, *right*) as highlighted by oil red O staining (*inset*), poorly differentiated tumors with a solid growth pattern (*bottom*, *left*), and a pseudoglandular pattern (*bottom*, *right*). (*C*) Summary of tumor incidence in *Albumin-Cre;Dicer1*$^{loxP/loxP}$ mice. Note that 12-month-old mice with tumors include 3 mice that died from HCCs at 9–11 months of age.

Recent studies have established that microRNAs are frequently deregulated in many types of cancers, including HCCs.[21,22] Some evidence suggests that the dominant role of microRNA processing during transformation may be tumor suppression. Lu et al reported that microRNAs are predominantly down-regulated in human tumors, and Kumar et al showed that the simultaneous deletion of *Dicer1* and expression of activated K-ras enhances lung tumorigenesis.[21,23] The dysregulated expression of fetal liver genes in *Dicer1*-deficient hepatocytes is intriguing considering the notion that cancers mimic corresponding fetal tissue, a hypothesis that is supported by the common expression of a group of genes referred to as oncofetal genes.[24,25] The reactivation of fetal stage–specific genes is also a common finding in human HCCs. α-Fetopro-

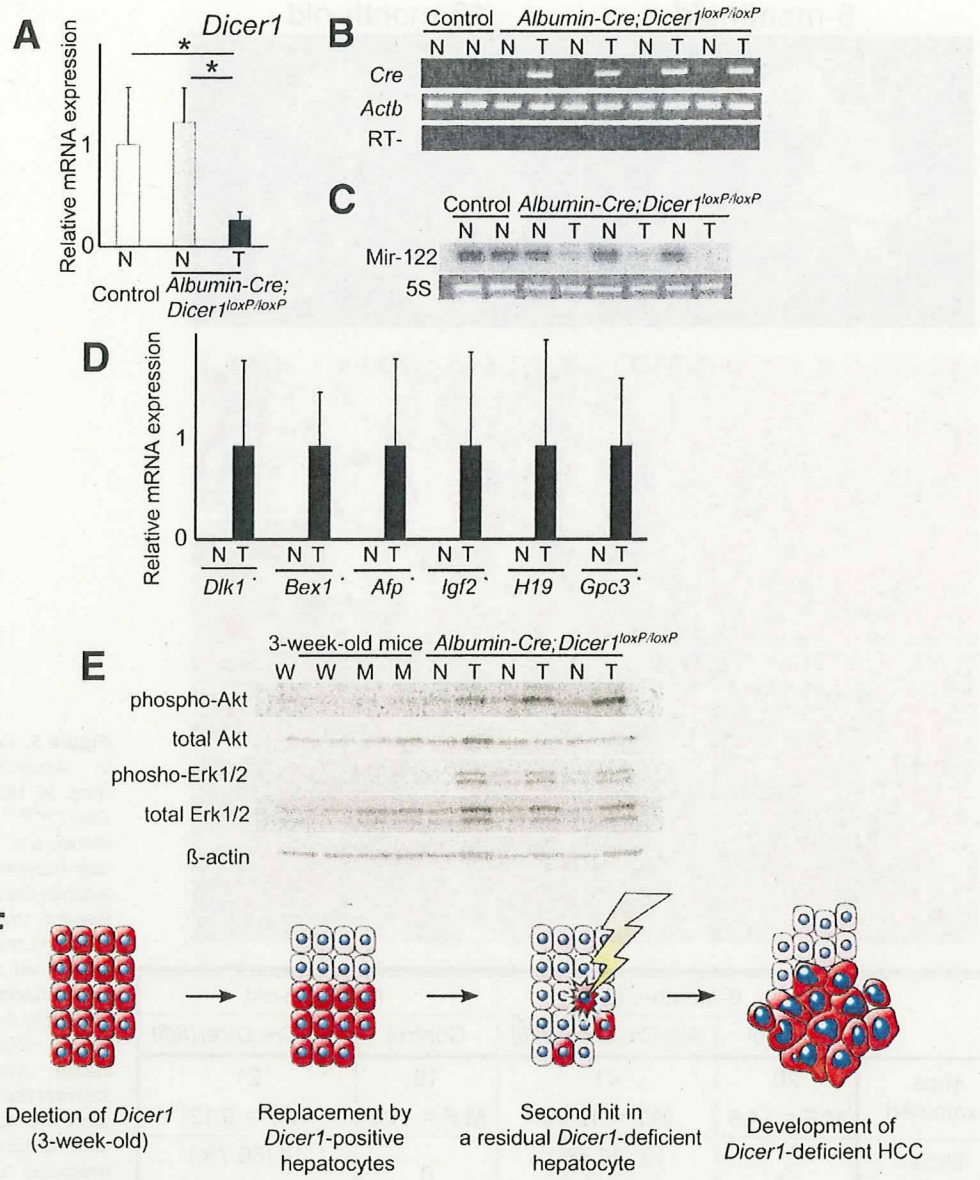

Figure 6. HCCs in *Albumin-Cre;Dicer1*$^{loxP/loxP}$ mice are derived from *Dicer1*-deficient hepatocytes. (*A*) Expression of *Dicer1* in nonneoplastic and tumor samples of control and *Albumin-Cre;Dicer1*$^{loxP/loxP}$ mice (n = 5–6 for each group). Messenger RNA expression was determined by quantitative PCR. Values are expressed as mean ± SD. $^{*}P < .05$. T, tumor; N, nonneoplastic liver tissue. (*B*) Reverse-transcription PCR analysis of *Cre* transgene expression. *Actb* served as a positive control. (*C*) Northern blot for mir-122. Ethidium bromide staining of 5S RNA served as a loading control. (*D*) Quantitative PCR analysis of oncofetal genes (n = 5–6 for each group). (*E*) Expression of phospho-Erk and phospho-Akt in HCCs and *Dicer1*-deficient livers. Protein samples from HCCs, corresponding nonneoplastic liver, and 3-week-old *Dicer1*-deficient and control livers were treated with the indicated antibodies. (*F*) Model of hepatocarcinogenesis in *Albumin-Cre;Dicer1*$^{loxP/loxP}$ mice. *Albumin-Cre;Dicer1*$^{loxP/loxP}$ mice exhibit the efficient deletion of *Dicer1* at 3 weeks after birth. However, *Dicer1*-deficient hepatocytes (*red cells*) gradually undergo apoptosis and *Dicer1*-expressing wild-type hepatocytes (*pink cells*) that have escaped Cre-mediated recombination repopulate the entire liver over time. When a *Dicer1*-deficient hepatocyte acquires secondary oncogenic stimuli presumably through additional genetic alterations, the absence of *Dicer1* cooperatively promotes the development of HCC.

tein, encoded by *AFP*, is the most widely used serum marker of HCCs in clinical practice.[26,27] Glypican-3, which is a gene product of *GPC3*, is another increasingly recognized serum and histologic marker of human HCCs.[28,29] Not only are these oncofetal genes known as tumor markers, several of their gene products, including delta-like 1, glypican-3, and insulin-like growth factor 2, have been implicated in the malignant potential of HCCs.[30–32] For instance, insulin-like growth factor 2 is a highly potent mitogen, and the

suppression of this gene alone has therapeutic benefits in a mouse implantation model of HCC.[30]

It is also notable that *Dicer1*-deficient liver showed increased expression of cell cycle–promoting genes, which is another common feature of HCCs. Even though we cannot exclude that these changes represent secondary effects such as a consequence of dysregulated fetal gene expression, it is tempting to speculate that these growth-promoting genes are controlled by a microRNA-mediated machinery. Of note, *Ccng1*, which is up-regulated also in *Dicer1*-deficient liver, has been identified as a direct target of mir-122.[4,8] Thus, *Dicer1*-deficient hepatocytes exhibit some characteristics consistent with transformed hepatocytes, including dysregulation of fetal liver genes and increased expression of cell cycle–promoting genes. However, the fact that *Dicer1*-deficient hepatocytes undergo apoptosis indicates that these changes are not sufficient to initiate tumorigenesis by themselves.

Our observations indicate that the disruption of *Dicer1* primarily impairs hepatocyte survival; however, it also promotes hepatocarcinogenesis in cells that escape the initial wave of cell death. Although these opposing effects of *Dicer1* loss on nonneoplastic hepatocytes and HCCs appear paradoxical, our findings are consistent with previous experimental observations. Impaired microRNA processing has resulted in reduced proliferative activity, tissue degeneration, or senescence in a variety of types of primary cells.[1–3,23,33–35] On the other hand, deletion of *Dicer1* promoted cellular transformation in the presence of activated K-ras both in vitro and in vivo.[23] Interestingly, it is known that the introduction of prototypical oncogenes into normal cells can induce apoptosis.[36,37] In these situations, the presence of appropriate survival signals can circumvent the apoptotic reaction and transform the cells.[37–39] Thus, the opposing effects of *Dicer1* loss on cell survival and transformation may somehow simulate those of oncogenes.

The fact that only a minor subset of *Dicer1*-deficient hepatocytes gives rise to HCCs suggests the requirement of a "second hit" that promotes hepatocarcinogenesis in *Dicer1*-deficient hepatocytes. We found that *Dicer1*-deficient HCCs consistently exhibited phosphorylation of Erk1/2 and Akt, processes that are also common in human HCCs.[40,41] Because nonneoplastic *Dicer1*-deficient livers did not show the activation of Erk1/2 or Akt, these events are not an immediate consequence of *Dicer1* loss but are acquired during tumorigenesis. Some secondary events leading to the activation of these pathways might be involved in the transformation of *Dicer1*-deficient hepatocytes and may promote hepatocarcinogenesis synergistically with the loss of *Dicer1* (Figure 6*F*).

The present study revealed novel and pivotal roles of *Dicer1* in hepatocyte survival, metabolism, developmental gene regulation, and tumor suppression in the liver. Reactivation of the fetal gene expression program might be a key mechanism of hepatocarcinogenesis induced by the loss of *Dicer1*. Because *Dicer1* is essential for microRNA processing, the phenotypes observed here would reflect the regulatory roles of microRNAs in the liver. Further studies will examine the functions of individual microRNAs to elucidate the precise mechanisms for the regulation of liver function by Dicer.

Supplementary Data

Note: To access the supplementary material accompanying this article, visit the online version of *Gastroenterology* at www.gastrojournal.org, and at doi: 10.1053/j.gastro.2009.02.067.

References

1. Harfe BD, McManus MT, Mansfield JH, et al. The RNaseIII enzyme Dicer is required for morphogenesis but not patterning of the vertebrate limb. Proc Natl Acad Sci U S A 2005;102:10898–10903.
2. Murchison EP, Partridge JF, Tam OH, et al. Characterization of Dicer-deficient murine embryonic stem cells. Proc Natl Acad Sci U S A 2005;102:12135–12140.
3. Kanellopoulou C, Muljo SA, Kung AL, et al. Dicer-deficient mouse embryonic stem cells are defective in differentiation and centromeric silencing. Genes Dev 2005;19:489–501.
4. Esau C, Davis S, Murray SF, et al. miR-122 regulation of lipid metabolism revealed by in vivo antisense targeting. Cell Metab 2006;3:87–98.
5. Krutzfeldt J, Rajewsky N, Braich R, et al. Silencing of microRNAs in vivo with 'antagomirs'. Nature 2005;438:685–689.
6. Grimm D, Streetz KL, Jopling CL, et al. Fatality in mice due to oversaturation of cellular microRNA/short hairpin RNA pathways. Nature 2006;441:537–541.
7. Ladeiro Y, Couchy G, Balabaud C, et al. MicroRNA profiling in hepatocellular tumors is associated with clinical features and oncogene/tumor suppressor gene mutations. Hepatology 2008;47:1955–1963.
8. Gramantieri L, Ferracin M, Fornari F, et al. Cyclin G1 is a target of miR-122a, a microRNA frequently down-regulated in human hepatocellular carcinoma. Cancer Res 2007;67:6092–6099.
9. Calabrese JM, Seila AC, Yeo GW, et al. RNA sequence analysis defines Dicer's role in mouse embryonic stem cells. Proc Natl Acad Sci U S A 2007;104:18097–18102.
10. Postic C, Shiota M, Niswender KD, et al. Dual roles for glucokinase in glucose homeostasis as determined by liver and pancreatic beta cell-specific gene knock-outs using Cre recombinase. J Biol Chem 1999;274:305–315.
11. Sekine S, Gutierrez P, Lan B, et al. Liver specific loss of beta-catenin results in delayed hepatocyte proliferation after partial hepatectomy. Hepatology 2007;45:361–368.
12. Obernosterer G, Martinez J, Alenius M. Locked nucleic acid-based in situ detection of microRNAs in mouse tissue sections. Nat Protoc 2007;2:1508–1514.
13. Sharov AA, Dudekula DB, Ko MS. A web-based tool for principal component and significance analysis of microarray data. Bioinformatics 2005;21:2548–2549.
14. Dennis G Jr, Sherman BT, Hosack DA, et al. DAVID: Database for Annotation, Visualization, and Integrated Discovery. Genome Biol 2003;4:P3.
15. Barad O, Meiri E, Avniel A, et al. MicroRNA expression detected by oligonucleotide microarrays: system establishment and expression profiling in human tissues. Genome Res 2004;14:2486–2494.

16. Clotman F, Lannoy VJ, Reber M, et al. The onecut transcription factor HNF6 is required for normal development of the biliary tract. Development 2002;129:1819–1828.
17. Sandgren EP, Palmiter RD, Heckel JL, et al. Complete hepatic regeneration after somatic deletion of an albumin-plasminogen activator transgene. Cell 1991;66:245–256.
18. Overturf K, Al-Dhalimy M, Tanguay R, et al. Hepatocytes corrected by gene therapy are selected in vivo in a murine model of hereditary tyrosinaemia type I. Nat Genet 1996;12:266–273.
19. Grompe M, Laconi E, Shafritz DA. Principles of therapeutic liver repopulation. Semin Liver Dis 1999;19:7–14.
20. Lagos-Quintana M, Rauhut R, Yalcin A, et al. Identification of tissue-specific microRNAs from mouse. Curr Biol 2002;12:735–739.
21. Lu J, Getz G, Miska EA, et al. MicroRNA expression profiles classify human cancers. Nature 2005;435:834–838.
22. Calin GA, Croce CM. MicroRNA signatures in human cancers. Nat Rev Cancer 2006;6:857–866.
23. Kumar MS, Lu J, Mercer KL, et al. Impaired microRNA processing enhances cellular transformation and tumorigenesis. Nat Genet 2007;39:673–677.
24. Uriel J. Cancer, retrodifferentiation, and the myth of Faust. Cancer Res 1976;36:4269–4275.
25. Alexander P. Foetal "antigens" in cancer. Nature 1972;235:137–140.
26. Taketa K. Alpha-fetoprotein: reevaluation in hepatology. Hepatology 1990;12:1420–1432.
27. Johnson PJ. The role of serum alpha-fetoprotein estimation in the diagnosis and management of hepatocellular carcinoma. Clin Liver Dis 2001;5:145–159.
28. Zhu ZW, Friess H, Wang L, et al. Enhanced glypican-3 expression differentiates the majority of hepatocellular carcinomas from benign hepatic disorders. Gut 2001;48:558–564.
29. Capurro M, Wanless IR, Sherman M, et al. Glypican-3: a novel serum and histochemical marker for hepatocellular carcinoma. Gastroenterology 2003;125:89–97.
30. Yao X, Hu JF, Daniels M, et al. A methylated oligonucleotide inhibits IGF2 expression and enhances survival in a model of hepatocellular carcinoma. J Clin Invest 2003;111:265–273.
31. Huang J, Zhang X, Zhang M, et al. Up-regulation of DLK1 as an imprinted gene could contribute to human hepatocellular carcinoma. Carcinogenesis 2007;28:1094–1103.
32. Capurro MI, Xiang YY, Lobe C, et al. Glypican-3 promotes the growth of hepatocellular carcinoma by stimulating canonical Wnt signaling. Cancer Res 2005;65:6245–6254.
33. Damiani D, Alexander JJ, O'Rourke JR, et al. Dicer inactivation leads to progressive functional and structural degeneration of the mouse retina. J Neurosci 2008;28:4878–4887.
34. Wang Y, Medvid R, Melton C, et al. DGCR8 is essential for microRNA biogenesis and silencing of embryonic stem cell self-renewal. Nat Genet 2007;39:380–385.
35. Koralov SB, Muljo SA, Galler GR, et al. Dicer ablation affects antibody diversity and cell survival in the B lymphocyte lineage. Cell 2008;132:860–874.
36. Evan GI, Wyllie AH, Gilbert CS, et al. Induction of apoptosis in fibroblasts by c-myc protein. Cell 1992;69:119–128.
37. Pelengaris S, Khan M, Evan GI. Suppression of Myc-induced apoptosis in beta cells exposes multiple oncogenic properties of Myc and triggers carcinogenic progression. Cell 2002;109:321–334.
38. Strasser A, Harris AW, Bath ML, et al. Novel primitive lymphoid tumours induced in transgenic mice by cooperation between myc and bcl-2. Nature 1990;348:331–333.
39. Jacobs JJ, Scheijen B, Voncken JW, et al. Bmi-1 collaborates with c-Myc in tumorigenesis by inhibiting c-Myc-induced apoptosis via INK4a/ARF. Genes Dev 1999;13:2678–2690.
40. Nakanishi K, Sakamoto M, Yamasaki S, et al. Akt phosphorylation is a risk factor for early disease recurrence and poor prognosis in hepatocellular carcinoma. Cancer 2005;103:307–312.
41. Schmidt CM, McKillop IH, Cahill PA, et al. Increased MAPK expression and activity in primary human hepatocellular carcinoma. Biochem Biophys Res Commun 1997;236:54–58.

Received July 9, 2008. Accepted February 19, 2009.

Reprint requests

Address requests for reprints to: Shigeki Sekine, MD, PhD, Pathology Division, National Cancer Center Research Institute, 5-1-1, Tsukiji, Chuo-ku, Tokyo, Japan. e-mail: ssekine@ncc.go.jp; fax: (81) 3-3248-2463; or Matthias Hebrok, PhD, Diabetes Center, Department of Medicine, University of California San Francisco, 613 Parnassus Avenue, HSW1112, Box 0540, San Francisco, California 94143. e-mail: mhebrok@ucsf.edu; fax: (415) 564-5813.

Acknowledgments

The authors thank Shigeru Tamura for photographic assistance, Fumio Hasegawa for electron microscopy, and John P. Morris IV for critical reading of the manuscript.

Conflicts of interest

The authors disclose no conflicts.

Funding

Supported by a Grant-in-Aid for the Third Term Comprehensive 10-Year Strategy for Cancer Control and a Grant-in-Aid for Cancer Research from the Ministry of Health, Labor and Welfare of Japan, as well as a program for promotion of Fundamental Studies in Health Sciences of the National Institute of Biomedical Innovation (NiBio), Japan. Work in M.H.'s laboratory was supported by a grant from the National Institutes of Health (CA112537).

Supplementary Table 1. Primary Antibodies Used in the Present Study

Antigen	Clone	Application	Dilution	Source
Phospho-histone H3	Polyclonal #9701	IHC-P	1:500	Cell Signaling Technology (Danvers, MA)
Cleaved caspase-3	Polyclonal #9661	IHC-P	1:500	Cell Signaling Technology
Cytokeratin 19	TROMA-III	IHC-P	1:5000	Developmental Studies Hybridoma Bank (Iowa City, IA)
TER-119	TER-119	IHC-P	1:100	BioLegend (San Diego, CA)
CD31	390	IHC-Fr	1:100	Biolegend
CD41	MWReg30	IHC-Fr	1:100	eBioscience (San Diego, CA)
ERK1/2	Polyclonal #9102	WB	1:1000	Cell Signaling Technology
Phospho-ERK1/2	Polyclonal #4377	WB	1:1000	Cell Signaling Technology
AKT	Polyclonal #9272	WB	1:250	Cell Signaling Technology
Phospho-AKT	Polyclonal #9271	WB	1:250	Cell Signaling Technology
β-Actin	AC-15	WB	1:3000	Sigma-Aldrich (St. Louis, MO)

IHC-P, immunohistochemistry (paraffin); IHC-Fr, immunohistochemistry (frozen); WB, Western blotting.

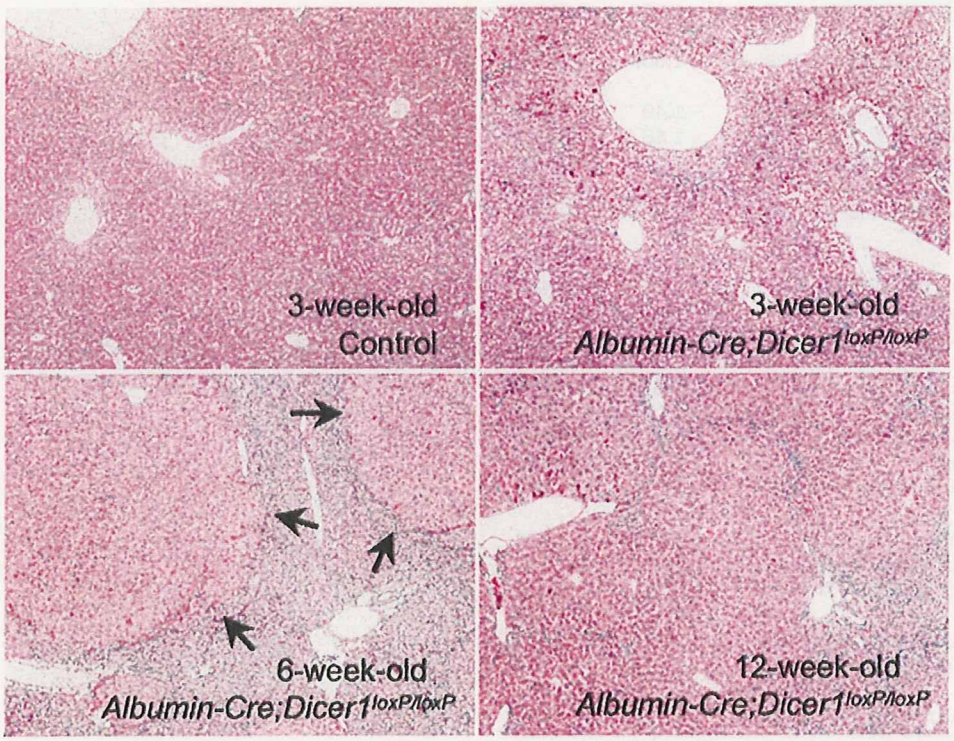

Supplementary Figure 1. Histology of control and *Albumin-Cre;Dicer1*$^{loxP/loxP}$ mouse livers during young adulthood. At 3 weeks of age, both control and *Albumin-Cre;Dicer1*$^{loxP/loxP}$ mouse livers showed homogeneous appearance, even though hepatocytes of *Albumin-Cre;Dicer1*$^{loxP/loxP}$ mice showed abnormalities at cytologic levels (see Figure 3*A* for high-magnification images). At 6 weeks after birth, *Albumin-Cre;Dicer1*$^{loxP/loxP}$ livers displayed round nodules consisting of eosinophilic and enlarged hepatocytes (*arrows*) that correspond to normal-colored areas on gross examination (Figure 1*A*) and areas positive for mir-122 expression (Figure 1*E*). Normal-appearing hepatocytes largely replaced the parenchyma of 12-week-old *Albumin-Cre;Dicer1*$^{loxP/loxP}$ livers.

Supplementary Table 2. MicroRNAs Down-regulated in *Albumin-Cre;Dicer1$^{loxP/loxP}$* Mouse Livers

Probe name	Log2 ratio	False discovery rate
hsa-miR-192/mmu-miR-192/rno-miR-192	−4.274	1.70E-05
hsa-miR-122/mmu-miR-122/rno-miR-122	−4.271	6.30E-05
hsa-miR-194/mmu-miR-194/rno-miR-194	−4.271	8.40E-06
hsa-miR-215	−4.164	1.60E-05
hsa-miR-193a-3p/mmu-miR-193/rno-miR-193	−3.822	8.40E-06
hsa-miR-122*	−3.162	2.20E-05
hsa-miR-148a/mmu-miR-148a	−3.089	8.40E-06
mmu-miR-101b/rno-miR-101b	−2.922	5.90E-05
hsa-miR-22/mmu-miR-22/rno-miR-22	−2.801	8.40E-06
hsa-miR-802/mmu-miR-802	−2.722	8.40E-06
hsa-miR-378/mmu-miR-378/rno-miR-378	−2.505	8.40E-06
hsa-miR-365/mmu-miR-365/rno-miR-365	−2.282	2.00E-05
hsa-miR-30c/mmu-miR-30c/rno-miR-30c	−2.179	2.50E-05
hsa-miR-31/mmu-miR-31/rno-miR-31	−2.113	2.00E-05
hsa-miR-101/mmu-miR-101a/rno-miR-101a	−1.944	0.00019
hsa-miR-30a/mmu-miR-30a/rno-miR-30a	−1.913	5.90E-05
hsa-miR-30e/mmu-miR-30e/rno-miR-30e	−1.764	5.50E-05
hsa-miR-30b/mmu-miR-30b/rno-miR-30b-5p	−1.674	0.00019
hsa-miR-200a/mmu-miR- 200a/rno-miR-200a	−1.617	0.00033
hsa-miR-22*/mmu-miR-22*/rno-miR-22*	−1.519	7.90E-05
hsa-miR-130a/mmu-miR-130a/rno-miR-130a	−1.508	6.60E-05
hsa-miR-200b/mmu-miR-200b/rno-miR-200b	−1.506	0.00034
hsa-miR-20a/mmu-miR-20a/rno-miR-20a	−1.49	0.00015
hsa-miR-29c/mmu-miR-29c/rno-miR-29c	−1.48	0.00018
hsa-miR-29a/mmu-miR-29a/rno-miR-29a	−1.471	0.00015
hsa-miR-19b/mmu-miR-19b/rno-miR-19b	−1.434	2.00E-04
hsa-miR-17/mmu-miR-17/rno-miR-17-5p/rno-miR-17	−1.415	0.00021
hsa-miR-106a	−1.401	0.00024
hsa-let-7f/mmu-let-7f/rno-let-7f	−1.277	0.00021
hsa-let-7a/mmu-let-7a/rno-let-7a	−1.25	0.00015
hsa-miR-30d/mmu-miR-30d/rno-miR-30d	−1.247	0.00016
mmu-let-7g	−1.241	0.00019
mmu-let-7f/rno-let-7f	−1.204	2.00E-04
mmu-let-7d/rno-let-7d	−1.167	0.00021
hsa-miR-107/mmu-miR-107/rno-miR-107	−1.163	0.00027
mmu-let-7a/rno-let-7a	−1.142	0.00021
hsa-miR-30e*/mmu-miR-30e*/rno-miR-30e*	−1.114	0.00027
hsa-let-7d/mmu-let-7d/rno-let-7d	−1.113	0.00034
hsa-miR-19a/mmu-miR-19a/rno-miR-19a	−1.107	0.0015
hsa-miR-185/mmu-miR-185/rno-miR-185	−1.088	0.00045
mmu-miR-20b	−1.087	0.00034
hsa-miR-26b/mmu-miR-26b/rno-miR-26b	−1.054	0.00028
hsa-miR-93/mmu-miR-93/rno-miR-93	−1.034	0.0011
rno-miR-352	−1.031	0.00034
hsa-miR-191/mmu-miR-191/rno-miR-191	−1.005	0.00034

NOTE. Probes that showed more than 2-fold changes with a false discovery rate <0.05 are listed.

Supplementary Table 3. MicroRNAs Up-regulated in *Albumin-Cre;Dicer1$^{loxP/loxP}$* Mouse Livers

Probe name	Log2 ratio	False discovery rate
mmu-miR-327	2.327	0.00019
mmu-miR-434-3p/rno-miR-434	1.589	0.0011
hsa-miR-142-3p/mmu-miR-142- 3p/rno-miR-142-3p	1.522	0.0011
hsa-miR-142-5p/mmu-miR-142 -5p/rno-miR-142-5p	1.321	0.00037
hsa-miR-199a-3p/hsa-miR-199b-3p/mmu-miR-199a-3p/mmu-miR-199b/rno-miR-199a-3p	1.162	0.00034
mmu-miR-434-5p	1.153	0.0035
hsa-miR-199a-5p/mmu-miR-199a-5p/rno-miR-199a-5p	1.15	0.0029
mmu-miR-199b*	1.104	0.002
hsa-miR-223/mmu-miR-223/rno-miR-223	1.057	0.00034

NOTE. Probes that showed more than 2-fold changes with a false discovery rate <0.05 are listed.